Multiple Bonds between Metal Atoms in Ordered Assemblies. 2. Quadruple Bonds in the Mesomorphic State[1]

David V. Baxter,*[,2a] Roger H. Cayton,[2b] Malcolm H. Chisholm,*[,2b] John C. Huffman,[2c] Elena F. Putilina,[2b] Sandra L. Tagg,[2b] Jodi L. Wesemann,[2b] Josef W. Zwanziger,*[,2b] and Frank D. Darrington[2d]

Contribution from the Departments of Chemistry and Physics and the Molecular Structure Center, Indiana University, Bloomington, Indiana 47405. and AMOCO Research Center. Naperville, Illinois 60566

*Received July 14, 1993. Revised Manuscript Received December 8, 1993**

Abstract: Various compounds of formula $M_2(O_2CR)_4$, where M = Cr, Mo, and W, have been synthesized, and their thermal behavior has been investigated. In the solid state they share a common laddered structure wherein one $M_2(O_2CR)_4$ unit is weakly associated with its neighbors through the agency of intermolecular M···O bonds. For M = W and R = *n*-Pr, the cell parameters at −171 °C are a = 8.867(9) Å, b = 10.934(14) Å, c = 5.563(6) Å, α = 100.01(4)°, β = 108.02(3)°, γ = 79.58(4)°, Z = 1, d_{calcd} = 2.38 g cm^{-3}, and space group $P\bar{1}$. Upon heating, the tungsten-containing compounds either undergo a simple crystal-to-isotropic liquid phase transition or decompose. The $Mo_2(O_2C(CH_2)_nCH_3)_4$ compounds have crystalline, liquid crystalline (mesomorphic), and isotropic liquid phases when n = 3–9. The related $Cr_2(O_2C(CH_2)_nCH_3)_4$ compounds show crystal-to-liquid crystal transitions but do not clear to isotropic liquids before decomposing at around 300 °C. The different thermotropic behavior of the Cr-, Mo-, and W-containing compounds is traced to the relative strength of the M···O intermolecular interactions that are preserved in the mesophase. The introduction of a branched chain lowers the crystal-to-liquid crystal phase transition, while the introduction of perfluorinated *n*-alkyl or para-*n*-alkyl or -alkoxy C_6H_4 groups raises the crystal-to-liquid crystal transition temperature. The phase changes (for several compounds) are reversible (enantiotropic) and have been characterized by differential scanning calorimetry. The mesophases of the $Mo_2(O_2CR)_4$ compounds reveal fan-shaped birefringent textures characteristic of discotic hexagonal disordered (D_{hd}) liquid crystalline arrangements. Variable temperature X-ray diffraction (XRD) studies were performed on $Mo_2(O_2C(CH_2)_nCR)_4$ for n = 3, 4, 6, and 7. The polycrystalline XRD patterns revealed triclinic cells with very similar values of c = *ca.* 5.6 Å, corresponding to the repeat unit of the polymer $[Mo_2(O_2CR)_4]_\infty$. In the mesophase the XRD patterns are dominated by a relatively intense peak at an angle below 10° in 2θ (Cu Kα). With increasing n, the d-spacing corresponding to this peak increases and is in all cases between the a and b lattice constants. For n = 6, two very much weaker peaks were found at 8.15 and 7.05 Å, corresponding to $1/\sqrt{3}$ and 1/2 of the main peak at 14.1 Å. These peaks confirm the hexagonal packing of the discotic columns. In addition, a broad band corresponding to 4.7 Å was seen, which is consistent with the expected average layer spacing along the columnar axis. An estimation of the coherence length within a column is *ca.* 30 Å, and thus the XRD pattern of the mesophase confirms the assignment D_{hd}. ^{13}C NMR studies employing $Mo_2(O_2{}^{13}C(CH_2)_6CH_3)_4$ allowed the determination of the chemical shift principal tensor elements of the carboxylate carbon by use of cross-polarization followed by high-powered proton decoupling. Comparison of the ^{13}C NMR spectra obtained for the isotropic liquid, the liquid crystalline phase, and the polycrystalline sample shows that the Mo–Mo axis is aligned perpendicularly to the magnetic field in the mesophase, consistent with the known large negative anisotropy of the magnetic susceptibility associated with the Mo–Mo bond.[4]

Introduction

The field of liquid crystal science has found numerous applications ranging from optoelectronics[3] to medicine.[4] It has been estimated that the worldwide market for LCDs will be upward of 2 trillion yen by the year 2000.[5] To date, all applications of liquid crystal technology involve organic molecules, and in most instances these have evolved through the synthetic and physical studies of manmade materials. It seems likely that metal ions will provide a pivotal role in future developments of liquid crystal technology just as they play key roles in nature's macromolecular assemblies.[6] Metal ions may be incorporated as guests within an existing organic assembly or may, by virtue of their unique coordination requirements, determine the architecture and structure of the mesophase. Metal ions have a wide variety of tunable properties to offer a macromolecular system. In particular, transition-metal ions exhibit variable redox behavior and may harvest or emit photons, in addition to carrying a number of unpaired electrons at a given center. Therefore, one can anticipate that metal-containing liquid crystals (metallomesogens) might exhibit useful optical, magnetic, and/or electronic properties. The study of metallomesogens is, however, relatively young, and many of the types of compounds examined so far have been patterned after organic analogues. For example, planar molecules such as metal-containing phthalocyanines,[7] porphyrins,[8] and β-diketonates[9] with long attendant side chains show thermotropic mesogenic behavior, as do related planar organic molecules (see Figure 1).

* Abstract published in *Advance ACS Abstracts*, February 15, 1994.

(1) Cayton, R. H.; Chisholm, M. H.; Huffman, J. C.; Lobkovsky, E. B. *J. Am. Chem. Soc.* **1991**, *113*, 8709.

(2) (a) Department of Physics. (b) Department of Chemistry. (c) The Molecular Structure Center. (d) AMOCO Research Center.

(3) (a) Heilmeier, G. H.; Zanoni, L. A.; Barton, L. A. *Appl. Phys. Lett.* **1968**, *13*, 46. (b) Williams, R. *J. Chem. Phys.* **1963**, *39*, 384. (c) Allen, G. *Chem. Ind. (London)* **1984**, *19*, 689.

(4) Crissey, J. T.; Fergason, J. L.; Bettenhausen, J. M. *J. Invest. Dermatol.* **1965**, *45*, 329.

(5) *The Economist* **1992**, (Feb 1), 79.

(6) (a) Bertini, I.; Drago, R. S.; Luchinat, C., Eds. *The Coordination Chemistry of Metalloenzymes*; Reidel: Dordrecht, 1983. (b) Martell, A. E., Ed. *Inorganic Chemistry in Biology and Medicine*; ACS Symposium Series 140; American Chemical Society: Washington, DC, 1980.

0002-7863/94/1516-4551$04.50/0

Dinuclear compounds with M–M multiple bonds exhibit a fascinating molecular chemistry and provide interesting monomeric units for macromolecular synthesis. In the first part of this series[1] we explored some of the prospects for the synthesis of 1D polymers incorporating M–M quadruple bonds of the type shown in **I** and **II** below.

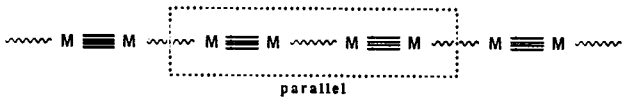

I

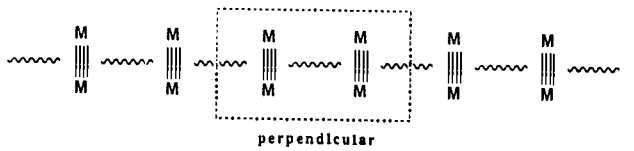

II

The redox potentials for the M$\overset{4}{-}$M bond are tunable by over 2 V and, depending upon the organic link, may form redox-active conducting or charge-insulating polymers. The alignment of the M–M axis with respect to the polymer axis in **I** and **II** rests upon the well-defined coordination chemistry of the M_2 subunit and the choice of organic bridge.

In principle, the alignment of a M$\overset{4}{-}$M unit could easily be achieved in a liquid crystal with or without the assistance of organic linkages since the susceptibility of the M$\overset{4}{-}$M bond is highly anisotropic. For example, the anisotropy of the magnetic susceptibility for the M$\overset{4}{-}$M bond is *ca.* -8000×10^{-36} m^3/molecule, which may be compared with -340×10^{-36} m^3/molecule for ethyne.[13] The ordering of the M$\overset{4}{-}$M axes is of interest with respect to the optical properties of the mesophase since the third-order coefficient for the nonlinear optical response, γ, in $Mo_2(O_2C\text{-}t\text{-}Bu)_4$ is known to be more than 5 times as large as that in ethyne.[14]

The dimetal tetracarboxylates of chromium,[15] molybdenum,[16] and tungsten[17] share a common paddle-wheel or lantern-type $M_2(O_2C)_4$ core and in the solid state, in the absence of neutral donor ligands, form extended laddered structures as a result of intermolecular oxygen-to-metal bonding as shown in **III** below.

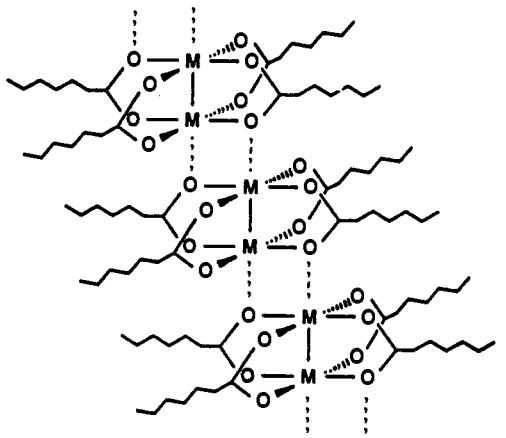

III

This structural motif seemed ideal for the observance of thermotropic mesomorphism, and in this paper we describe our initial studies that were prompted by this line of reasoning. It should also be noted that related dinuclear carboxylates of copper,[18] rhodium,[19] and ruthenium[20] have been shown to exhibit thermotropic mesophases. Compounds with M–M triple bonds, such as the $M_2(OR)_6$ compounds,[21] are also suitable candidates, as can be judged from the packing of the cyclohexyl rings in the structure of the $W_2(O\text{-}c\text{-}C_6H_{11})_6$ molecule shown in **IV** below. However, in this paper we restrict our attention to $M_2(O_2CR)_4$ compounds where M is a group VI metal.

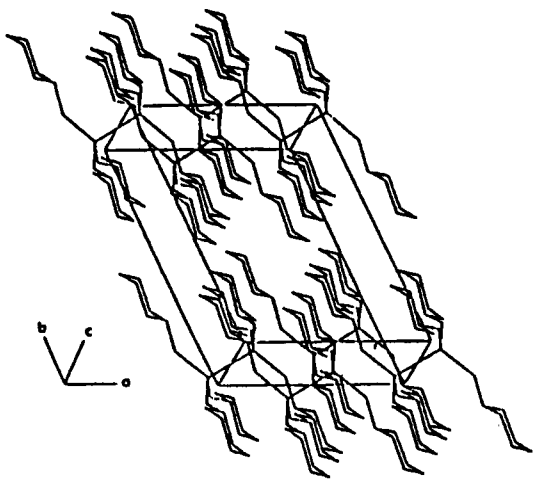

IV

Results and Discussion

Synthesis of Compounds. (a) Chromium. The dichromium tetracarboxylates were prepared from the reactions between anhydrous chromium(II) chloride and the sodium salt of the appropriate carboxylic acid[22] in methanol according to eq 1.

(7) (a) Cho, I.; Lim, Y. *Mol. Cryst. Liq. Cryst.* **1988**, *154*, 9. (b) Piechocki, C.; Simon, J.; Skoulios, A.; Guillon, D.; Weber, P. *J. Am. Chem. Soc.* **1982**, *104*, 5245.

(8) (a) Gregg, B. A.; Fox, M. A.; Bard, A. J. *J. Am. Chem. Soc.* **1989**, *111*, 3024. (b) Gaspard, S.; Maillard, P.; Billard, J. *Mol. Cryst. Liq. Cryst.* **1985**, *123*, 369. (c) Ohta, K.; Watanabe, T.; Fujimoto, T.; Yamamoto, I. *J. Chem. Soc., Chem. Commun.* **1989**, 1611.

(9) (a) Mehrotra, R. C.; Bohra, R.; Gaur, D. P. *Metal β-Diketonates and Allied Derivatives*; Academic Press: London, 1978. (b) Sakashita, H.; Nishitani, A.; Sumiya, Y.; Terauchi, H.; Ohta, K.; Yamamoto, I. *Mol. Cryst Liq. Cryst.* **1988**, *163*, 211.

(10) Schubert, H.; Lorenz, H.-J.; Hoffmann, R.; Franke, F. *Z. Chem.* **1966**, *6*, 337.

(11) Cotrait, M.; Gaultier, J.; Polycarpe, C.; Giroud, A.-M.; Mueller-Westerhoff, U. T. *Acta Crystallogr.* **1983**, *C39*, 833.

(12) van der Pol, J. F.; Nelleman, E.; Zwikker, J. W.; Nolte, R. J. M.; Drenth, W.; Aerts, J.; Visser, R.; Picken, S. J. *Liq. Cryst.* **1989**, *6*, 577.

(13) (a) San Filippo, J., Jr. *Inorg. Chem.* **1972**, *11*, 3140. (b) Cotton, F. A.; Kitagawa, S. *Polyhedron* **1988**, *7*, 1673. (c) In this paper we use SI units, in which magnetic susceptibilities are expressed in m^3/molecule. Susceptibilities in centimeter–gram–second (cgs) units may be converted to SI units by multiplication by $4\pi \times 10^{-6}$/N. Note also that in SI units the McConnell equation for the excess chemical shift due to the susceptibility of neighboring molecular fragments includes a factor of 4π in the denominator.

(14) Hopkins, M. D., personal communication.

(15) Cotton, F. A.; Rice, C. E.; Rice, G. W. *J. Am. Chem. Soc.* **1977**, *99*, 4704.

(16) Cotton, F. A.; Mester, Z. C.; Webb, T. R. *Acta Crystallogr.* **1974**, *B30*, 2768.

(17) Sattelberger, A. P.; McLaughlin, K. W.; Huffman, J. C. *J. Am. Chem. Soc.* **1981**, *103*, 2880.

(18) (a) Abied, H.; Guillon, D.; Skoulios, A.; Weber, P.; Giroud-Godquin, A.-M.; Marchon, J.-C. *Liq. Cryst.* **1987**, 269. (b) Takeoshi, M.; Watanabe, N.; Tamanushi, B. *Colloid Polym. Sci.* **1978**, *256*, 588.

(19) (a) Giround-Godquin, A.-M.; Marchon, J.-C.; Guillon, D.; Skoulios, A. *J. Phys. Chem.* **1986**, *90*, 5502. (b) Poizat, O.; Strommen, D. P.; Maldivi, P.; Giroud-Godquin, A.-M.; Marchon, J.-C. *Inorg. Chem.* **1990**, *29*, 4851.

(20) Marchon, J.-C.; Maldivi, P.; Giroud-Godquin, A.-M.; Guillon, D.; Skoulios, A.; Strommen, D. P. *Philos. Trans. R. Soc. London* **1990**, *A330*, 109.

(21) Chisholm, M. H.; Folting, K.; Hampden-Smith, M.; Smith, C. A. *Polyhedron* **1987**, *6*, 1747.

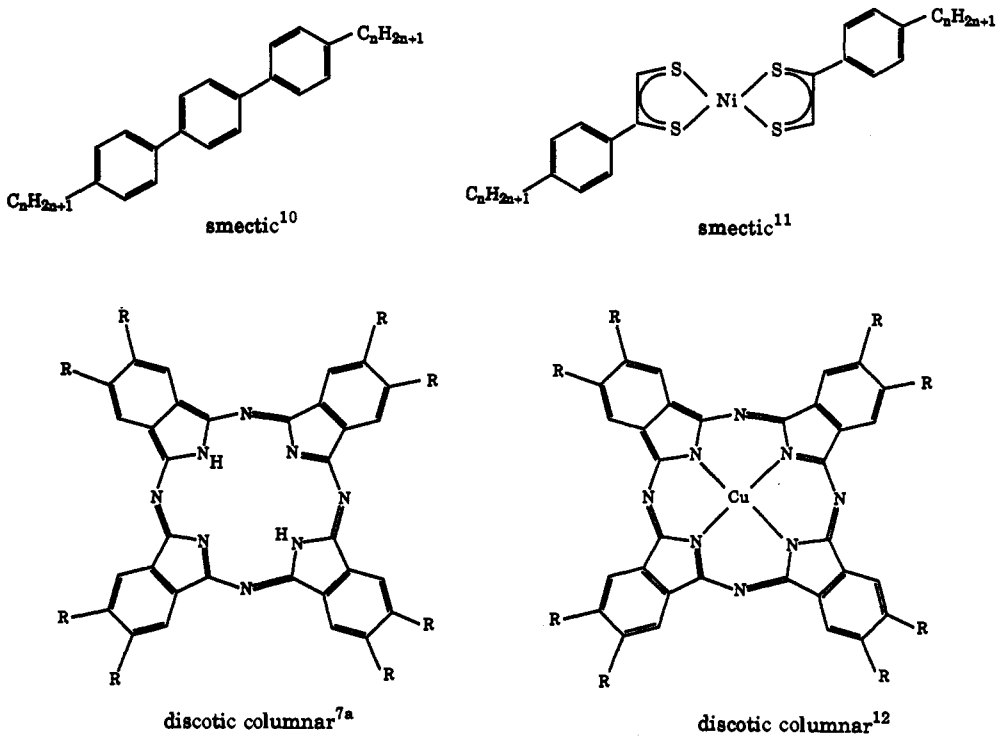

Figure 1. Structural relationships between some typical organic and metalloorganic classes of molecules that have been shown to exhibit thermotropic mesophases.

$$2CrCl_2 + 4NaO_2CR \xrightarrow[MeOH]{\text{room temperature}} Cr_2(O_2CR)_4 + 4NaCl \quad (1)$$

In reaction 1 the sky blue chromium(II) chloride solution in MeOH yielded colored precipitates $Cr_2(O_2CR)_4$ that were isolated by filtration and washed with excess methanol prior to drying under a dynamic vacuum. The $Cr_2(O_2CR)_4$ compounds range in color from tan (R = *p*-C_6H_4-*n*-C_7H_{15}) to purple (R = *n*-C_7F_{15}) and are extremely air-sensitive, being very readily oxidized to green Cr(III) complexes. The products were characterized by ^1H and ^{19}F NMR spectroscopy.

This method, eq 1, has the advantage over the reaction between Cp_2Cr and RCOOH (2 equiv)[23] because there is no possible excess acid that may coordinate to the Cr^{2+}-containing centers. Furthermore, it is simple and NaCl is readily removed by washing with MeOH.

(b) Molybdenum. Two methods have been employed in the synthesis of Mo_2^{4+}-containing tetracarboxylates. The first involves the well-known reaction between $Mo(CO)_6$ and an excess of a carboxylic acid under reflux in a high boiling solvent such as diglyme,[24] eq 2.

$$2Mo(CO)_6 + >4RCOOH \xrightarrow[diglyme]{\text{reflux}} Mo_2(O_2CR)_4 + 12CO + 2H_2 \quad (2)$$

In reaction 2, the introduction of a few milliliters of THF (THF = tetrahydrofuran) prevents the usual frustration of $Mo(CO)_6$ subliming onto the cooler parts of the reaction vessel and the condenser. Reaction 2 involves the oxidatively-induced dimerization of molybdenum and has only one distinct synthetic problem. It is necessary to employ an excess of the carboxylic acid, which at the end of the reaction must be removed to yield pure $Mo_2(O_2CR)_4$ compounds. This requires the application of a dynamic vacuum with heating to remove high boiling carboxylic acids and the diglyme. (In certain cases the $Mo_2(O_2C(CH_2)_nCH_3)_4$ compounds crystallize from the mother liquor.) Subsequent purification by recrystallization from hexane is possible.

An alternative procedure involving the exchange of carboxylate ligands[25] was also employed as outlined in eq 3.

$$Mo_2(O_2CMe)_4 + 4.5RCOOH \xrightarrow[toluene]{\text{reflux}} Mo_2(O_2CR)_4 + 4MeCOOH \quad (3)$$

In eq 3, the slight excess of added carboxylic acid was used to drive the reaction to completion along with the removal of the more volatile acetic acid as an azeotrope with toluene.

All the $Mo_2(O_2CR)_4$ compounds were various shades of yellow and were the least air-sensitive of the series (M = Cr, Mo, W), although precautions were taken to keep O_2 and moisture away from both solids and solutions of these compounds.

(c) Tungsten. The ditungsten tetracarboxylates, in which the carboxylate was octanoate or perfluorooctanoate, were prepared from $W_2(O_2CMe)_4$ according to the procedure analogous to that given in eq 3. $W_2(O_2CMe)_4$ cannot be obtained from the reaction between $W(CO)_6$ and MeCOOH but is prepared from the reaction between $W_2Cl_4(THF)_4$ and NaOAc in THF, which is analogous

(22) (a) Ocone, L. R.; Block, B. P. *Inorg. Synth.* **1966**, *8*, 125. (b) Sharrock, P.; Théophanides, T.; Brisse, F. *Can. J. Chem.* **1973**, *51*, 2963.
(23) (a) Cotton, F. A.; Extine, M. W.; Rice, G. W. *Inorg. Chem.* **1978**, *17*, 176. (b) Cotton, F. A.; Rice, G. W. *Inorg. Chim. Acta* **1978**, *27*, 75.
(24) Stephenson, T. A.; Bannister, E.; Wilkinson, G. *J. Chem. Soc.* **1964**, 2538.
(25) (a) Holste, G. Z. *Anorg. Allg. Chem.* **1975**, *414*, 81. (b) Cotton, F. A.; Norman, J. G., Jr. *J. Coord. Chem.* **1971**, *1*, 161. (c) Cotton, F. A.; Norman, J. G., Jr.; Stults, B. R.; Webb, T. R. *J. Coord. Chem.* **1976**, *5*, 217. (d) Mureinik, R. J. *J. Inorg. Nucl. Chem.* **1976**, *38*, 1275.

to the method of Sattelberger[26] for the preparation of $W_2(O_2C$-t-$Bu)_4$. However, in the preparation of the n-butyrate, where it was desirable to obtain crystals suitable for X-ray crystallography, we employed the reductive elimination of ethane and ethene[27] as shown in eq 4.

$$1,2\text{-}W_2Et_2(NMe_2)_4 + 4n\text{-}PrCOCOOC\text{-}n\text{-}Pr \xrightarrow[\text{hexane}]{\text{room temperature}} W_2(O_2C\text{-}n\text{-}Pr)_4 + 4n\text{-}PrCONMe_2 + C_2H_6 + C_2H_4 \quad (4)$$

All the $W_2(O_2CR)_4$ compounds are air-sensitive, yellow or yellow-orange materials. $W_2(O_2C$-n-$C_7F_{15})_4$ was yellow below 0 °C but slowly decomposed at room temperature.

(d) $Mo_2(S_2CR)_4$, Where R = n-C_3H_7 and n-C_7H_{15}. The dithiocarboxylates were prepared from the reaction between the specific n-alkyl Grignard reagent and carbon disulfide in THF at 0 °C. The resulting magnesium dithiocarboxylate was used in a metathetic reaction with $Mo_2(O_2CMe)_4$ according to eq 5.

$$n\text{-}R\text{-}MgBr + CS_2(2\text{ equiv}) \xrightarrow[\text{THF}]{0\,^\circ C} n\text{-}RCS_2MgBr \quad (5a)$$

$$4n\text{-}RCS_2MgBr + Mo_2(O_2CMe)_4 \xrightarrow[\text{THF/MeOH}]{\text{room temperature}} Mo_2(S_2C\text{-}n\text{-}R)_4 + 4MeCO_2MgBr \quad (5b)$$

In reaction 5a, MeOH is added subsequently to induce precipitation of the shiny, metallic orange, air-stable $Mo_2(S_2C$-n-$R)_4$ compounds. We were unsuccessful in obtaining single crystals suitable for single crystal X-ray diffraction studies of either compound (R = n-C_3H_7 or n-C_7H_{15}) in the absence of axial donor ligands. The compounds $Mo_2(S_2CR)_4$·2THF, where R = Me and Ph, have been previously characterized by Cotton and co-workers.[28]

Observations of Phase Transitions. If a polycrystalline sample of a $M_2(O_2CR)_4$ compound is heated in a sealed capillary tube and viewed under magnification, as is typical in a melting point determination apparatus, the transition from crystal to the liquid crystalline phase is observed as wetting of the sample. The sample is seen to lose crystallinity, to shrink, and to remain as a free-standing column within the capillary. The clearing temperature (liquid crystal-to-isotropic liquid transition) is detected by the transformation of the viscous column to a free-flowing transparent liquid. The reverse phase change, isotropic liquid-to-liquid crystalline phase, yields a noncrystalline opaque material.

None of the chromium carboxylates showed a clearing point prior to decomposition at *ca.* 300 °C. The tungsten compounds, on the other hand, showed only a simple melting and did not reveal a mesophase. In the cases of the perfluorooctanoates of both chromium and tungsten, the complexes decomposed in the solid state prior to any phase transition.

By far the most interesting was the $Mo_2(O_2CR)_4$ series, because these compounds allowed access to all three phases as a function of R. We were therefore able to study the influence of R upon the phase transition temperatures and also to examine the liquid crystalline phases by polarized microscopy upon cooling from the isotropic liquids.[29]

Phase Transitions in $Mo_2(O_2C(CH_2)_nCH_3)_4$ Compounds. The temperature dependence of phase transitions for chain lengths where n = 2–10 is depicted in Figure 2. Some of the compounds showed crystal-to-crystal transitions prior to the solid-to-mesophase transition. The thermotropic behavior was monitored by differential scanning calorimetry (DSC), and the enthalpy changes so determined are recorded in Table 1. All enthalpies reported are obtained for samples prepared by crystallization from hydrocarbon solvents, and the determined values are given

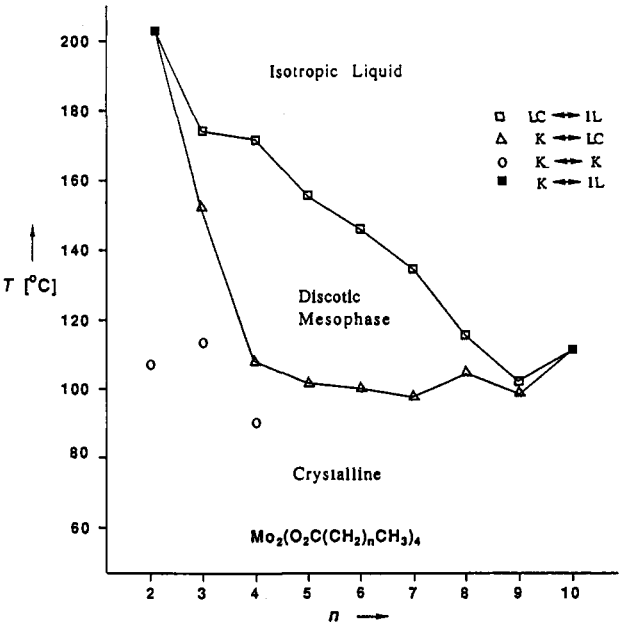

Figure 2. Phase/temperature profile for $Mo_2(O_2C(CH_2)_nCH_3)_4$ compounds where n = 2–10. LC = liquid crystal; K = crystal; IL = isotropic liquid.

Table 1. Phase Transition Temperatures (°C) and ΔH Values (kcal mol^{-1}) for $Mo_2(O_2C(CH_2)_nCH_3)_4$ Series

n	phase profile, temperature (ΔH)[a]
2	K ← 203 (5.2) → IL
3	K ← 152 (4.0) → LC ← 174 (0.6) → IL
4	K ← 108 (5.1) → LC ← 172 (0.6) → IL
5	K ← 101 (10.4) → LC ← 155 (0.6) → IL
6	K ← 100 (13.6) → LC ← 147 (0.6) → IL
7	K ← 98 (12.0) → LC ← 134 (0.4) → IL
8	K ← 105 (12.8) → LC ← 116 (0.3) → IL
9	K ← 99 (19.0) → LC ← 102 (0.2) → IL
10	K ← 111 (27.8) → IL

[a] K = crystal, LC = liquid crystal, IL = isotropic liquid. ΔH values accurate to 15%, temperatures to 2 °C.

(26) Santure, D. J.; Huffman, J. C.; Sattelberger, A. P. *Inorg. Chem.* **1985**, *24*, 371.
(27) Chisholm, M. H.; Chiu, H. T.; Huffman, J. C. *Polyhedron* **1984**, *3*, 759.
(28) Cotton, F. A.; Fanwick, P. E.; Niswander, R. H.; Sekutowski, J. C. *Acta Chem. Scand.* **1978**, *A32*, 663.
(29) Cayton, R. H.; Chisholm, M. H.; Darrington, F. D. *Angew. Chem., Int. Ed. Engl.* **1990**, *29*, 1481.

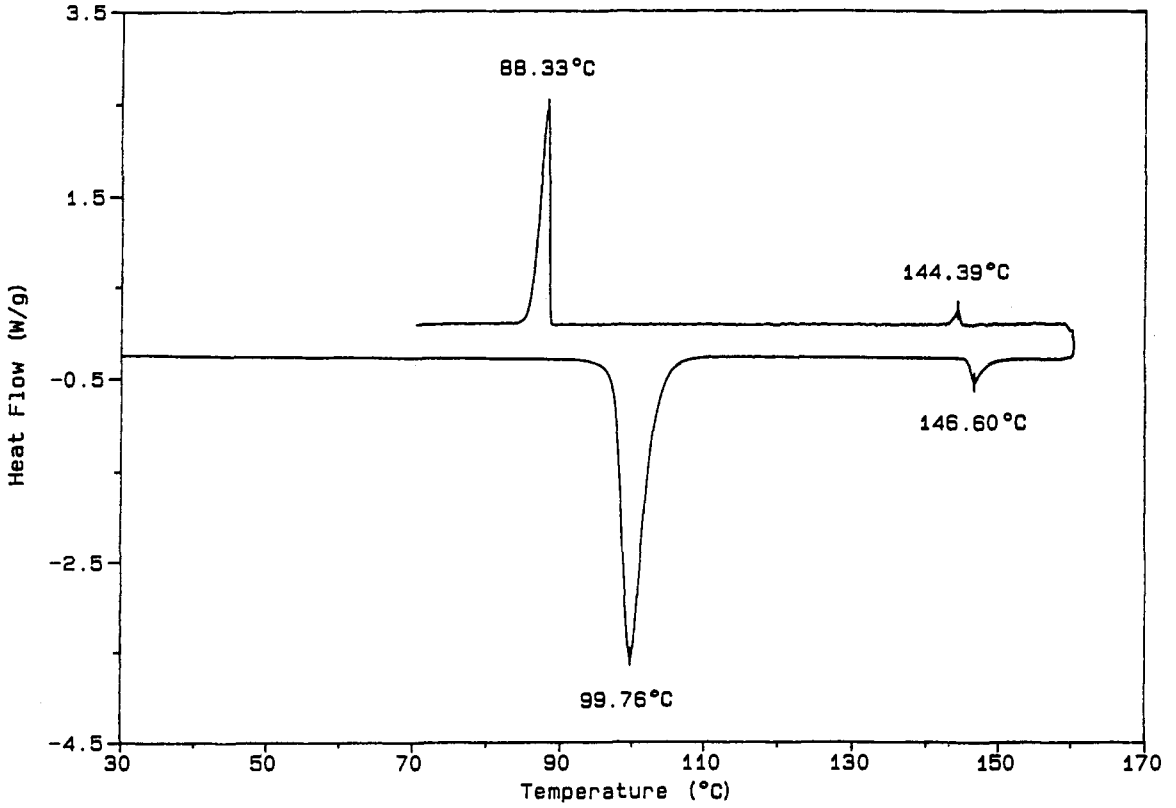

Figure 3. Differential scanning calorimetry (DSC) plot for $Mo_2(O_2C(CH_2)_6CH_3)_4$. The lower curve shows the heating profile with endotherms at 99.8 °C (K → LC) and 146.6 °C (LC → IL) for the phase changes obtained at a heating rate of 5 deg/min. The top curve reveals that the phase changes are reversible upon cooling.

for the heating cycle at 5 deg/min. Under an inert atmosphere the phase changes were reversible, and thus, for the series of compounds where n = 3–9, the phase behavior may be termed enantiotropic. A typical DSC cycle is shown in Figure 3.

The following points are worthy of note with respect to the phase behavior of $M_2(O_2C(CH_2)_nCH_3)_4$ compounds.

(1) For M = Ru, Rh, and Cu, similar behavior was observed with respect to solid-to-mesophase transitions, which typically occur at *ca.* 100 °C for $n > 3$. However, only for selected copper(II) *n*-alkanoates were clearing temperatures observed below 250 °C prior to decomposition.[30] The dimolybdenum tetra-*n*-alkanoates are unique in showing liquid crystal-to-isotropic liquid transitions for $3 \leq n \leq 9$.

(2) For M = W, we have not observed any mesophase. A transition from crystal to isotropic liquid occurs at 90 °C for n = 6.

(3) For M = Mo, the temperature range of the mesophase is larger for $4 \leq n \leq 7$ than for n = 3 or n = 8 and 9.

(4) For $n \geq 10$ and M = Mo, we have not observed the liquid crystalline phase—only a simple melting occurs upon heating the crystalline samples. For M = Ru, Rh, and Cu, the mesophase has been observed for n as large as 22.[30]

(5) The effect of odd n versus even n on the phase transitions is relatively small within the series of $Mo_2(O_2C(CH_2)_nCH_3)_4$ for n = 4–9 compared to a number of well-characterized series of *n*-alkyl-containing organic liquid crystalline materials.[31]

(6) The dichromium tetra-*n*-alkyl carboxylates show crystal-to-liquid crystal transitions, but upon further heating they decompose (*ca.* 300 °C) prior to a liquid crystal-to-isotropic liquid transition.

The key question raised by these observations is that of what is controlling the presence (or absence) and temperature range of the mesophase. At one time we considered the possibility that the mesophase was a result of the rupture of the weak intermolecular $M_2\cdots O$ interactions and that the side chains were mobile as depicted schematically below in V.

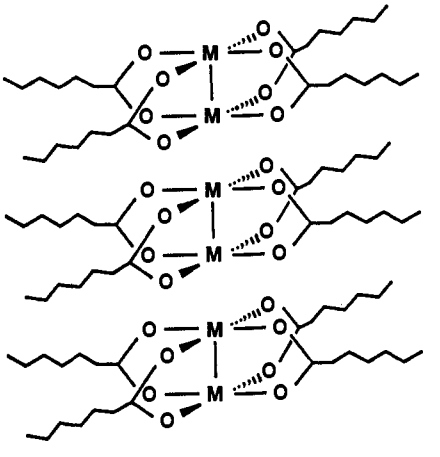

V

This behavior has to be ruled out on the basis of the thermal properties of the series of compounds for M = Cr, Mo, and W (summarized in Figure 7 and discussed later in this paper). As the identity of the metal changes, the strengths of the axial $M_2\cdots O$ interactions vary. The relative strengths of these interactions are inversely related to the strengths of the M–M bonds, though

(30) Abied, H.; Guillon, D.; Skoulios, A.; Giroud-Godquin, A.-M.; Maldivi, P.; Marchon, J.-C. *Colloid Polym. Sci.* **1988**, *266*, 579.

(31) (a) Eidenschink, R.; Erdmann, D.; Krause, J.; Pohl, L. *Angew. Chem., Int. Ed. Engl.* **1977**, *16*, 100. (b) Gray, G. W. *Advances in Liquid Crystal Materials for Applications*; BDH Publications, BDH Limited: Poole, England, 1978.

(32) Lindsey, A. J.; Wilkinson, G.; Motevalli, M.; Hursthouse, M. B. *J. Chem. Soc., Dalton Trans.* **1985**, 2321.

(33) Cotton, F. A.; Shiu, K.-B. *Rev. Chim. Min.* **1986**, *23*, 14.

(34) (a) Campbell, G. C.; Haw, J. F. *Inorg. Chem.* **1988**, *27*, 3706. (b) Lomer, T. R.; Perera, K. *Acta Crystallogr.* **1974**, *B30*, 2912. (c) Lomer, T. R.; Perera, K. *Acta Crystallogr.* **1974**, *B30*, 2913.

Table 2. Structural Comparisons among $M_2(O_2CR)_4$ Compounds

M	R	M—M (Å)	M—O (Å)	M···O (Å)	ΔM—O (Å)[a]	ref
Cr	CH_3	2.29	2.03	2.33	0.30	15
Mo	CH_3	2.09	2.12	2.65	0.53	16
W	C_2H_5	2.19	2.08	2.67	0.59	27
Ru[b]	CH_3	2.26	2.07	2.34	0.27	32
Rh	C_3H_7	2.37	2.03	2.34	0.31	33
Cu	C_3H_7	2.58	1.96	2.22	0.26	34a

[a] Δ(M—O) = (M···O) − (M—O). [b] With H_2O in the axial sites.

the latter are not known precisely. One way to estimate the relative strengths of these M_2···O interactions is to compare the structural parameters shown for a closely related series of compounds of formula $M_2(O_2CR)_4$, where M = Cr, Mo, W, Ru, Rh, and Cu and R is alkyl (see Table 2). To a first-order approximation, strong bonds may be correlated with short bonds, and the parameter Δ(M–O), defined as d(M···O) − d(M—O) in angstroms, can be seen to reveal the trend W > Mo > Cr > Rh > Ru > Cu. For Cu, the Cu–Cu distance of *ca.* 2.60 Å does not correspond to a formal M–M bond.

If the M_2···O interactions were not important, we would expect that compounds of formula $M_2(O_2C(CH_2)_nCH_3)_4$ would all show similar thermotropic behavior. If the M_2···O interactions were important and were broken when entering the mesophase, a situation corresponding to that shown in V, then, for a given value of n, we would expect to observe different temperatures for the crystal-to-mesophase transitions and similar temperatures for the mesophase-to-isotropic liquid transitions. Neither case occurs. When the value of Δ(M–O) is relatively small, the compounds do not show a mesophase-to-isotropic liquid transition temperature prior to decomposition in the temperature range 250–300 °C. However, for M = W, which has the largest value of Δ(M–O) and presumably the weakest M_2···O interaction, heating the crystalline sample causes only a crystal-to-isotropic liquid transition. For molybdenum, the intermolecular Mo_2···O interactions are just sufficiently strong to allow access to the mesophase for n = 3–9 and weak enough within this series to allow access to the isotropic liquid.

Although the intermolecular M_2···O interactions are important in the mesophase for M = Mo, these bonds are kinetically labile, being readily broken and formed, allowing for dynamic behavior described later on the basis of the X-ray and ^{13}C NMR studies. A pictorial representation of the mesophase is given in Figure 4.

Methods of Controlling the Thermotropic Phase Behavior in $M_2(O_2CR)_4$ Compounds. (a) Mixture Formulation. It is known that the transition temperatures of binary mixtures of mesogenic materials can be lower than those of either component.[35] Taking into account also that mixtures are always necessary to satisfy requirements for liquid crystal display technology, we studied the phase behavior of the mixture of two $Mo_2(O_2C(CH_2)_nCH_3)_4$ compounds where n = 6 and 7 as a function of molar composition.

The data were taken on a heating cycle of mixtures crystallized from a neat melt. The resulting graph of dependence of the phase behavior upon the molar ratio of the mixture is shown in Figure 5. A significant lowering of crystal-to-mesophase transition temperature was observed in all cases, with the minimum transition temperature of *ca.* 87 °C occurring in the range 50–66.6 mol % $Mo_2(O_2C(CH_2)_6CH_3)_4$. The clearing temperatures were found to vary less with composition.

The transition of a mixture can be relatively well predicted by the Schroder van Laar equation[36] from knowledge of the molar fractions, transition temperatures, and ΔH values. The theory is applicable for ideal solutions and immiscible solids. Based on the observed values of ΔH and transition temperatures, the Schroder van Laar equation predicts a eutectic point at a composition 45%, n = 6, and 55%, n = 7, with a temperature of 84 °C. Thus, within the limits of our experimental errors, the graph shown in Figure 5 seems a reasonable fit. However, this may be fortuitous for two reasons: (1) the dimetal centers are known to be kinetically labile toward carboxylate exchange,[37] and (2) there is no reason to believe that the ΔH of mixing is zero.

(b) Effects of Varying R on the Transition Temperatures. For various technological applications, it would be advantageous to have complete control over the phase temperature behavior for a given class of $M_2(O_2CR)_4$ compounds. Since we now know that the inorganic backbone of the $M_2(O_2CR)_4$ polymers, the

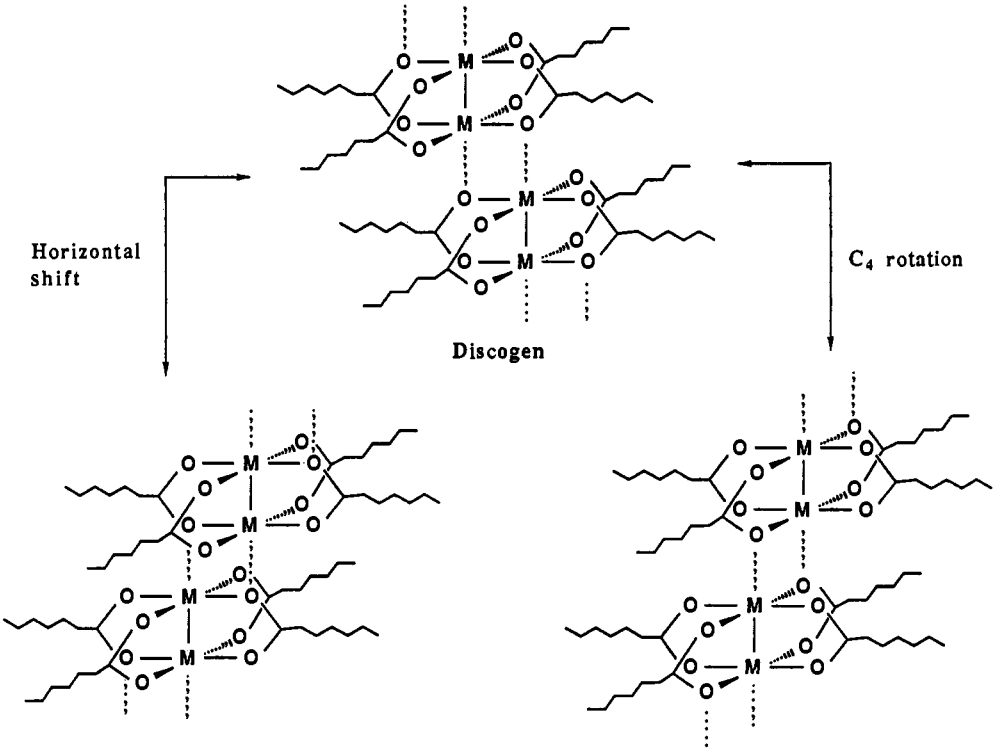

Figure 4. Pictorial representation of columnar stacking found in the mesophase. The spacing of 4.7 Å observed in the XRD corresponds to the average intermolecular separation within a column.

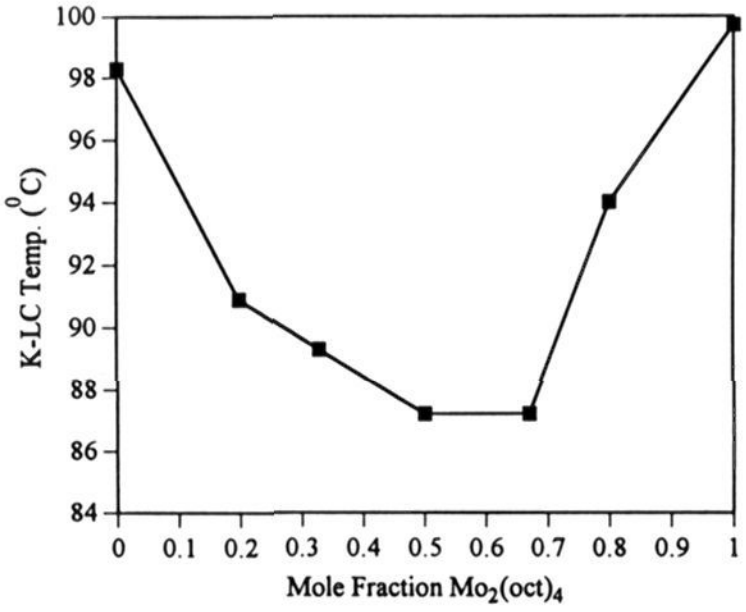

Figure 5. Temperature/mole fraction phase diagram showing the K → LC transition for mixtures of $Mo_2(O_2C(CH_2)_nCH_3)_4$ where n = 6 (oct) and 7.

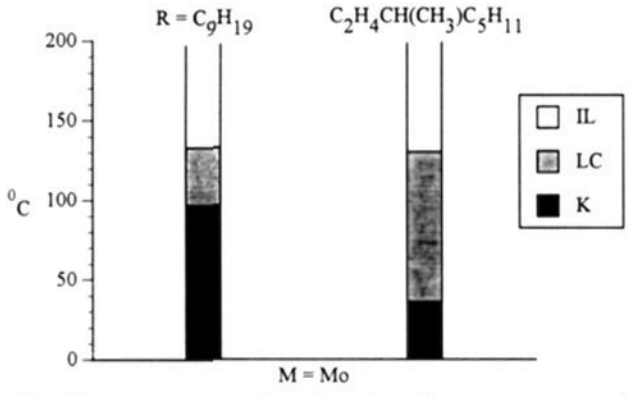

Figure 6. Bar diagram comparing the phase/temperature profiles for a straight-chain versus a branched-chain $Mo_2(O_2CR)_4$ compound. The open-ended bars denote that the compound is stable up to the indicated temperature.

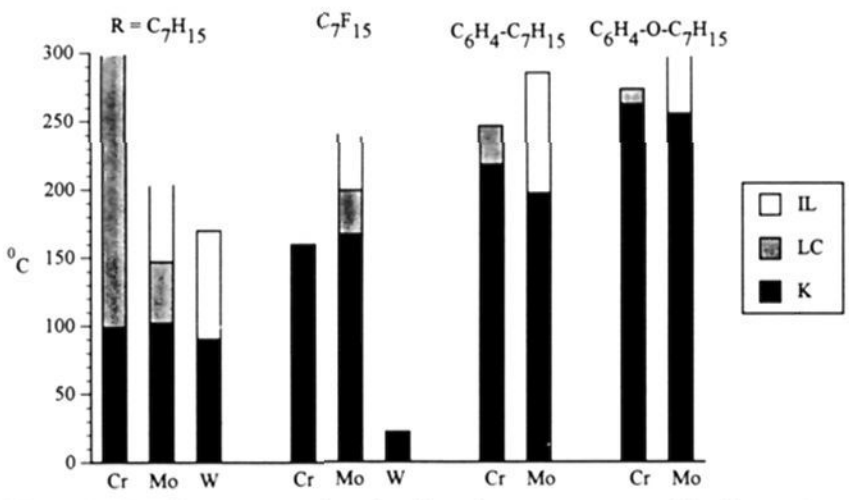

Figure 7. Bar diagram showing the phase/temperature profiles for various $M_2(O_2CR)_4$ compounds where M = Cr, Mo and W and R = n-alkyl, n-perfluoroalkyl, and para-substituted phenyl alkyl or ether derivatives. Open-ended bars denote that the compound is stable up to the indicated temperature. Closed-ended bars denote decomposition.

M_2···O interactions, controls access to the mesophase, we investigated the effects of variations in the properties of R, the organic substituents, on the phase behavior of the metallomesogens of chromium and molybdenum.

(i) Side-Chain Branching. It is known that side-chain branching in an alkyl chain often lowers the crystal-to-mesophase transition temperature without affecting the clearing temperature in organic molecules such as hexasubstituted benzenes.[38] We explored the influence of 4-methyl-nonanoate, $^-O_2C(CH_2)_2CH(CH_3)(CH_2)_4(CH_3)$, upon the phase behavior of the Cr_2- and Mo_2-containing compounds.[39] The results for the Cr_2-containing compound were inconclusive, in part, because of the air-sensitivity of the sample and also because a clearing point is not attained prior to thermal decomposition. For molybdenum, however, a straightforward comparison is possible for the 4-methyl nonanoate and the n-decanoate, and the data are summarized in the bar graph shown in Figure 6. Both compounds melt to isotropic liquids at *ca.* 120 °C, but the crystal-to-liquid crystal transition is lowered to about body temperature (37 °C) for the branched-chain compound. When studied by DSC, it is observed that on cooling the mesophase remains present at room temperature due to hysteresis effects similar to that shown in Figure 3. Forced cooling of the sample (immersion in liquid N_2) causes crystallization, and upon heating, the crystal-to-liquid crystal transition can again be observed.

(ii) Substitution of Fluorine for Hydrogen in the Alkyl Chain. Recognizing that the intermolecular M_2···O interactions are essential for attainment of the mesophase, we wondered whether the substitution of electron-withdrawing groups R would increase the Lewis acidity of the M_2^{4+} centers and thereby make weak axial interactions stronger. Conceivably one could make the W_2^{4+} tetracarboxylates show the mesophase, for example, and also increase the clearing temperature for the Mo_2^{4+}-containing compounds, making Mo_2^{4+} centers more like Cr_2^{4+}. To explore this possibility, the series $M_2(O_2C(CF_2)_6CF_3)_4$ for M = Cr, Mo, and W was prepared. The chromium and tungsten compounds proved thermally unstable, as noted in the Experimental Section. However, the Mo_2-containing compound exhibited enantiotropic phase behavior. As shown in Figure 7, the clearing temperature of the perfluorooctanoate was raised compared to the hydrocarbon analogue by *ca.* 50 °C to become close to 200 °C. The crystal-to-liquid crystal phase transition temperature was also raised by a similar amount. Presumably, the latter reflects upon the relative chain–chain attractive lattice forces—the weak van der Waals forces—in the crystalline state.

(iii) Substituted Aromatic Side Chains. n-Alkyl and n-alkyl ether aromatic molecules which have a "head" of a benzene ring and a long aliphatic "tail" are well known to show thermotropic liquid crystalline phases.[40] We therefore explored the use of O_2C-p-C_6H_4-O-n-C_7H_{15} and O_2C-p-C_6H_4-n-C_7H_{15} carboxylates for M = Cr and Mo. The comparison of the phase behavior is again shown in a bar diagram in Figure 7. In some ways these compounds may be viewed as derivatives of the $M_2(O_2C(CH_2)_6CH_3)_4$ compounds by the imaginary insertion of a phenyl or a phenoxy substituent at the head of the n-alkyl chain. Within this context, the crystal-to-liquid crystal or crystal-to-isotropic liquid phase transition is increased quite markedly, by approximately 100 °C for both M = Cr and Mo in the case of phenyl insertion and by *ca.* 150 °C for phenoxy insertion. This may be due to the more favorable hydrocarbon–hydrocarbon interactions associated with the aromatic rings. However, only the chromium compounds show a mesophase prior to thermal decomposition. The molybdenum compounds melt to isotropic liquids.

$Mo_2(S_2C$-n-$C_xH_{2x+1})_4$, Where x = 7 and 3. In order to explore the effect of substituting sulfur for oxygen, we prepared two dithiocarboxylate analogues of the n-alkanoates of dimolybdenum that showed a mesophase upon heating. $Mo_2(S_2C$-n-$C_7H_{15})_4$ showed only a crystal-to-isotropic liquid transition at *ca.* 180 °C and shortly above this temperature decomposed. Prior to melting, it showed crystal-to-crystal phase transitions. Initially, a single

(35) Bahadur, B., Ed. *Liquid Crystals. Applications and Uses*; World Scientific Publishing: 1990; p 129.

(36) (a) Hsu, E. C.-H.; Johnson, J. F. *Mol. Cryst. Liq. Cryst.* **1973**, *20*, 177. (b) Schroder, I. *Z. Phys. Chem.* **1893**, *11*, 449.

(37) The facile equilibrium $Mo_2(O_2C$-t-$Bu)_4 + Mo_2(O_2CCH_2$-t-$Bu)_4 \rightleftarrows Mo_2(O_2C$-$t$-$Bu)_{4-n}(O_2CCH_2$-$t$-$Bu)_n$, where n = 4–0, has been noted previously. Casas, J. M.; Cayton, R. H.; Chisholm, M. H. *Inorg. Chem.* **1991**, *30*, 358.

(38) Collard, D. M.; Lillya, C. P. *J. Am. Chem. Soc.* **1991**, *113*, 8577.

(39) The effect of side-chain branching upon the motion of the alkyl chains has been discussed for $Cu_2(O_2CR)_4$ compounds: Giroud-Godquin, A.-M.; Maldivi, P.; Marchon, J.-C.; Bée, M.; Carpentier, L. *Mol. Phys.* **1989**, *68*, 1367.

(40) (a) Finkenzeller, U.; Geelhaar, J.; Weber, G.; Pohl, L. *Liq. Cryst.* **1989**, *5*, 313. (b) Gray, G. W.; Harrison, K. J.; Nash, J. A. *Pramana Suppl.* **1975**, *1*, 381. (c) Sen, S.; Brahma, P.; Roy, S. K.; Mukherjee, D. K.; Roy, S. B. *Mol. Cryst. Liq. Cryst.* **1983**, *100*, 327.

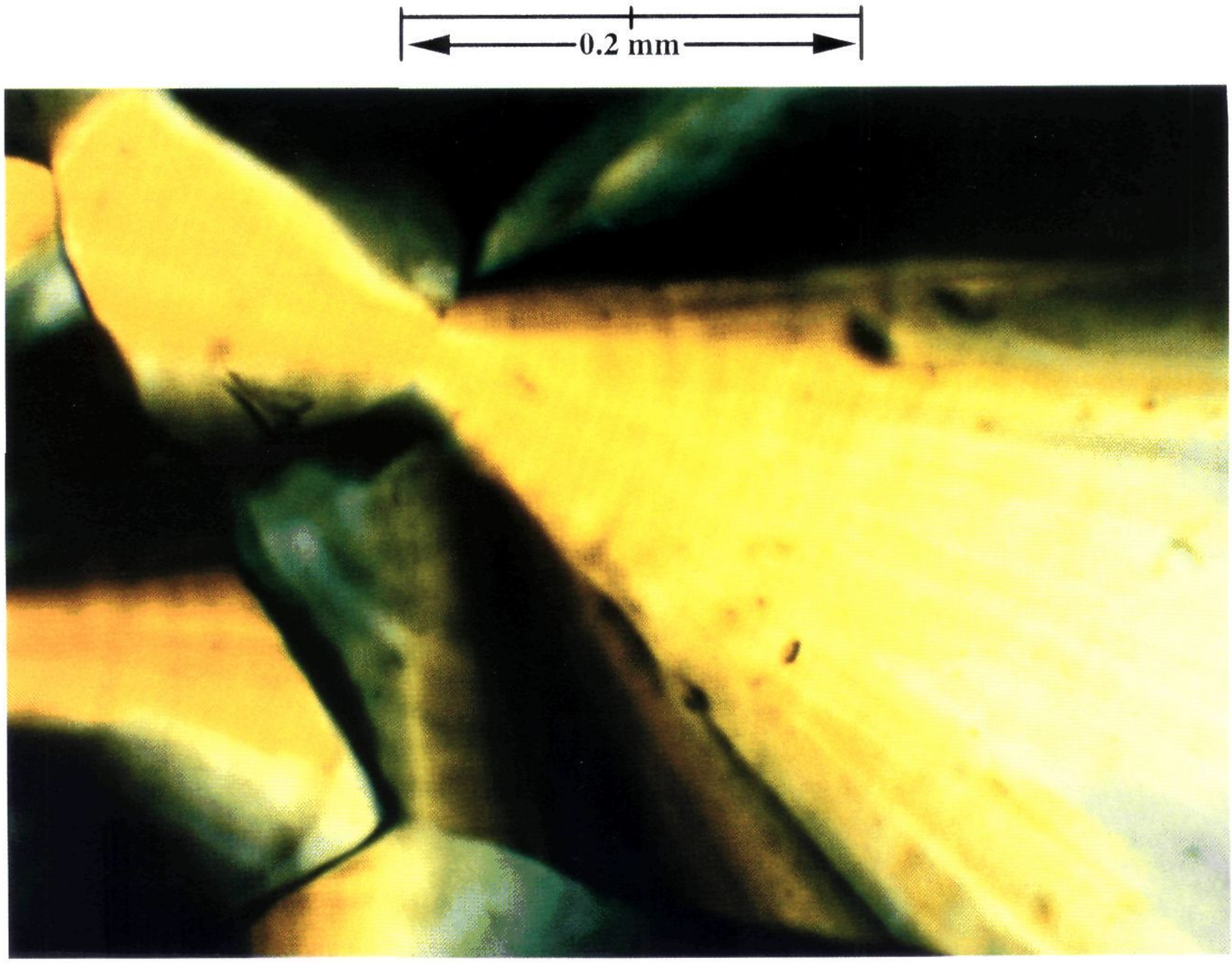

Figure 8. Photomicrograph for the mesophase of $Mo_2(O_2C(CH_2)_6CH_3)_4$ obtained upon cooling from the isotropic liquid. The polarizers were set at 90° to one another.

irreversible transition was observed at 134.4 °C (ΔH = 3.0 kcal/mol). (TGA studies showed that this was not due to loss of solvent.) Subsequent cycles revealed a reversible phase transition (crystal-to-crystal) at 56.8 °C (ΔH = 1.3 kcal/mol). Thus, the first phase is only accessible from crystallization from hydrocarbon solutions, while the second and third phases are only accessible from the solid phase. In any event, the mesophase was not observed for $Mo_2(S_2C\text{-}n\text{-}C_7H_{15})_4$, which most likely results from weaker axial donor interactions in the solid state in the case of sulfur versus oxygen. For example, while it is possible to obtain $Mo_2(O_2CPh)_4$ without axial solvent donor ligands, such as THF, the related dithiocarboxylates have always retained the O-donor solvent[28] in place of forming a laddered structure by way of sulfur-to-Mo_2 bonding. This may reflect the preference that the Mo_2^{4+}-center has for oxygen relative to sulfur. $Mo_2(S_2C\text{-}n\text{-}C_3H_7)_4$ did not exhibit a mesophase either and decomposed prior to melting at 223 °C.

Characterization of the Mesophases. (a) By Polarized Microscopy. A characteristic feature of liquid crystals is that they exhibit birefringence under polarized light. From the optical textures revealed in the photomicrographs, it is possible to classify the nature of the mesophase. It is important to recognize that the mesophase shows very different textures depending upon whether it is accessed by heating or cooling. In Figure 8 we show the photomicrograph of $Mo_2(O_2C(CH_2)_6CH_3)_4$ in its mesophase accessed by cooling. Upon cooling from the isotropic liquid, the mesophase grows like a crystal and therefore has straight boundaries and larger domains. The observed fan-shaped optical textures are characteristic of discotic mesophases. This type of discotic behavior might well have been anticipated on the basis of the schematic representation of the mesophase shown in Figure 4 which results from the ordering due to the maintenance of $Mo_2\cdots O$ intermolecular interactions.

Discotic mesogens can form a variety of phases: nematic, columnar, ordered or disordered, hexagonal or rectangular.[41] In our case the optical textures are most consistent with the presence of a hexagonal columnar phase, D_h, and the micrograph shown in Figure 8 may be compared specifically with that shown in Figure 5b in ref 42.

Organic compounds that show ordered and disordered hexagonal discotic mesophases include hexaalkoxytriphenylenes and truxenes.[43] The longer chain substituted compounds ($n > 10$ for the alkyl side chain) tend to be disordered, D_{hd}, rather than the ordered D_{ho}. The enthalpies of the phase transitions from D_{hd} to isotropic liquid are lower than those for the ordered, D_{ho}, and typically are around 0.3 kcal mol^{-1}.[42] These ΔH values are very similar to those found for the $Mo_2(O_2CR)_4$ compounds reported in this work (Table 1).

(41) Chandrasekhar, S. Liquid Crystals of Disk-like Molecules. *Philos. Trans. Rl. Soc. London* **1983**, *A309*, 93.

(42) Destrade, C.; Foucher, P.; Gasparoux, H.; Tinh, N. H.; Levelut, A. M.; Malthete, J. *Mol. Cryst. Liq. Cryst.* **1984**, *106*, 121.

(43) (a) Billard, J.; Dubois, J. C.; Nguyen, H. T.; Zann, A. *Nouv. J. Chim.* **1978**, *2*, 535. (b) Destrade, C.; Mondon, M. C.; Malthete, J. *J. Phys.* **1979**, *40*, *C3*, 17. (c) Foucher, P.; Destrade, C.; Malthete, J.; Nguyen, H. T. *9th International Liquid Crystal Conference*, Bangalore, 1982.

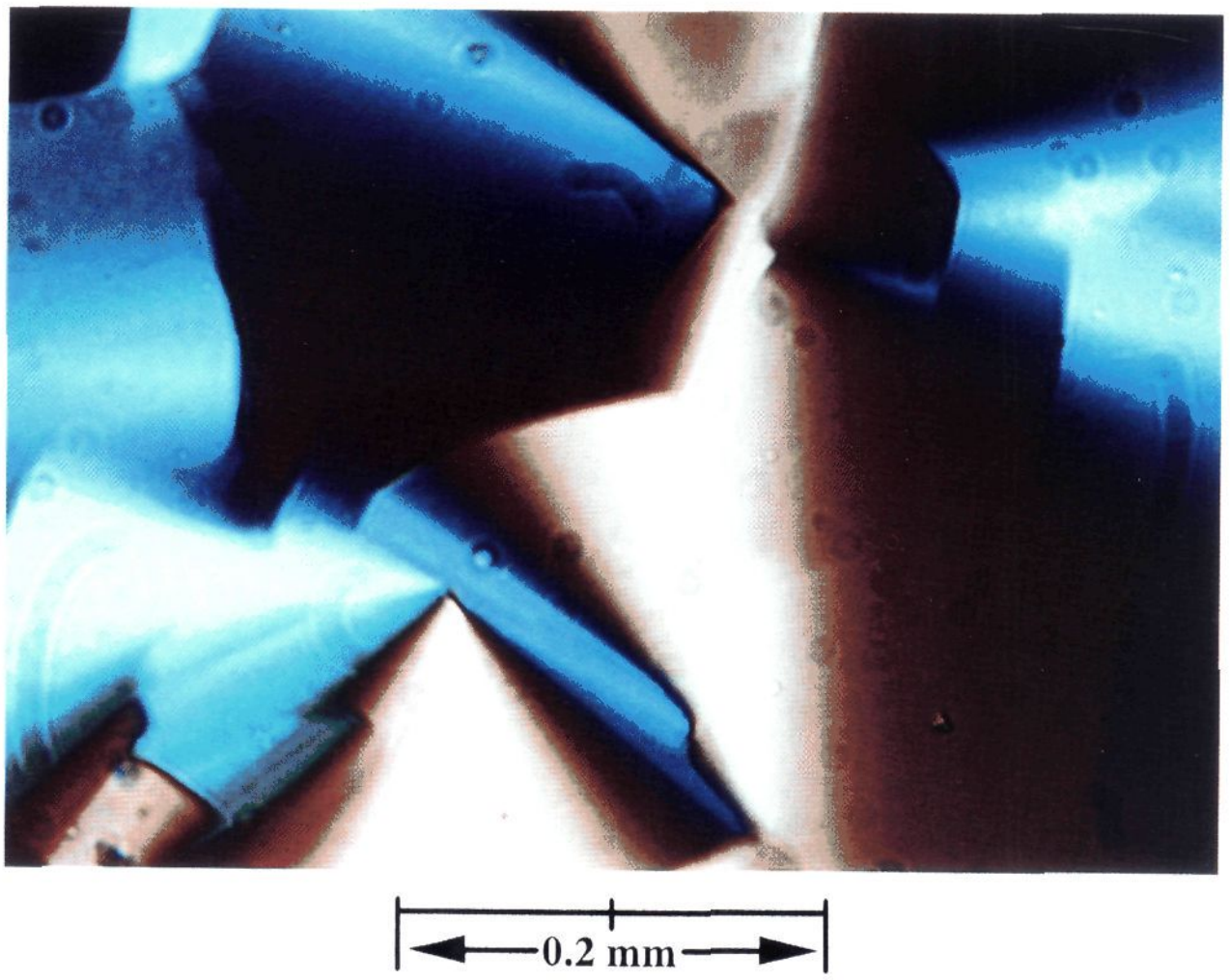

Figure 9. Photomicrograph of $Mo_2(O_2C(CF_2)_6CF_3)_4$ in the mesophase accessed upon cooling from the isotropic liquid. The polarizers were set at 90° to one another.

Table 3. Unit Cell Lattice Constant Distances for $M_2(O_2CR)_4$ Series Calculated from X-ray Powder Diffraction Patterns

		lattice constants (distances, Å)		
compound	cell type	*a*	*b*	*c*
$Mo_2(O_2C(CH_2)_2CH_3)_4$	tricl[d]	11.14 ± 0.04	8.856 ± 0.03	5.593 ± 0.017
$W_2(O_2C(CH_2)_2CH_3)_4$[a]	tricl	10.93 ± 0.01	8.867 ± 0.09	5.563 ± 0.006
$Mo_2(O_2C(CH_2)_3CH_3)_4$	tricl	13.59 ± 0.06	8.46 ± 0.03	5.604 ± 0.01
$Mo_2(O_2C(CH_2)_4CH_3)_4$	tricl	16.61 ± 0.03	8.642 ± 0.01	5.592 ± 0.007
$Mo_2(O_2C(CH_2)_6CH_3)_4$[b]	tricl	21.31 ± 0.03	8.593 ± 0.01	5.551 ± 0.006
$Mo_2(O_2C(CH_2)_6CH_3)_4$[c]	BCO[e]	25.66 ± 0.03	16.04 ± 0.01	14.047 ± 0.01
$Mo_2(O_2C(CH_2)_7CH_3)_4$[c]	tricl	24.67 ± 0.02	7.788 ± 0.004	5.558 ± 0.08
$Cu_2(O_2C(CH_2)_2H_3)_4$[a,34]	tricl	11.70 ± 0.003	8.806 ± 0.002	5.192 ± 0.002
$Cu_2(O_2C(CH_2)_6CH_3)_4$[34]	tricl	22.06	8.80	5.20
$Cu_2(O_2C(CH_2)_8CH_3)_4$[34]	tricl	28.13	7.94	5.28

[a] Data from single crystal X-ray diffraction measurements (unit cells have been reoriented to correspond to the unit cell convention of the diffraction patterns, $a > b > c$). [b] Crystallized from a neat melt. [c] Crystallized from hydrocarbon solvent. [d] Triclinic. [e] Body-centered orthorhombic.

$Mo_2(O_2C\text{-}n\text{-}C_7F_{15})_4$ showed very similar optical texture in its mesophase, as shown in Figure 9, and therefore we are inclined to the view that this also belongs to the discotic class of mesogens, D_{hd}.

(b) By X-ray Diffraction Studies. A number of compounds were studied by using X-ray diffraction in both the solid and liquid crystalline phases. At room temperature, compounds in the series $Mo_2(O_2C(CH_2)_nCH)_4$ (n = 2, 3, 4, 6, and 7) exhibit triclinic crystalline phases, with the smallest cell dimension virtually constant ($c \approx 5.6$ Å) throughout the series. This distance corresponds to the separation between Mo dimers along the polymerization direction. Tables 3 and 4 list the cell parameters found for this phase and show that a increases monotonically across the series while b remains relatively constant. In some cases (e.g., n = 4, 6, and 7), a second solid phase was found as well, but we were unable to index the powder pattern of the second phase in all cases.

As is evident in Figure 10, the XRD pattern for the mesophase is dominated by a relatively intense peak at an angle below 10° in 2θ (using Cu Kα radiation). With increasing n, the d-spacing corresponding to this peak increases, but in all cases studied (n = 3, 4, 6, and 7), the spacing lies between the a and b lattice constants of the triclinic solid phase (see Table 5). Two very much weaker peaks were found in the n = 6 sample at 8.15 and 7.05 Å. These correspond to $1/\sqrt{3}$ and 1/2 of the main peak (at 14.1 Å) and therefore confirm a hexagonal packing arrangement for the discotic columns in this sample. For this sample, a broad band corresponding to a distance of 4.7 Å is also visible. The hexagonal packing of the columns in the mesophase implies that in this phase the molecules do not remain in the uniform laddered structure shown in **III**.[44] Rather random motions,[45] such as those depicted in Figure 4, produce, on average, circular columns. Evidence for these motions, based on ^{13}C NMR measurements, is discussed below. Within this model for the columnar structure, the 4.7-Å spacing seen in the X-ray diffraction pattern is consistent with the expected average layer-to-layer separation along the columns. The presence of such a peak is sometimes taken to indicate a D_{ho} mesophase structure. In the present case, however, the breadth of the peak indicates a

(44) Chandrasekhar, S.; Ranganath, G. S. *Rep. Prog. Phys.* **1990**, *53*, 57.
(45) Giroud-Godquin, A.-M.; Marchon, J.-C.; Guillon, D.; Skoulios, A. *J. Phys. Lett.* **1984**, *45*, L681.

Table 4. Unit Cell Lattice Constant Angles for $M_2(O_2CR)_4$ Series Calculated from X-ray Powder Diffraction Patterns

compound	cell type	lattice constants (angles, deg) α	β	γ
$Mo_2(O_2C(CH_2)_2CH_3)_4$	tricl[d]	95.5 ± 0.3	89.7 ± 0.3	85.1 ± 0.3
$W_2(O_2C(CH_2)_2CH_3)_4$[a]	tricl	108.02 ± 0.3	100.01 ± 0.4	79.58 ± 0.4
$Mo_2(O_2C(CH_2)_3CH_3)_4$	tricl	97.0 ± 0.3	93.1 ± 0.3	83.6 ± 0.3
$Mo_2(O_2C(CH_2)_4CH_3)_4$	tricl	99.5 ± 0.2	90.3 ± 0.2	84.6 ± 0.2
$Mo_2(O_2C(CH_2)_6CH_3)_4$[b]	tricl	99.2 ± 0.2	89.16 ± 0:16	84.47 ± 0.11
$Mo_2(O_2C(CH_2)_6CH_3)_4$[c]	BCO[e]	90	90	90
$Mo_2(O_2C(CH_2)_7CH_3)_4$[c]	tricl	96.41 ± 0.15	86.7 ± 0.2	89.56 ± 0.1
$Cu_2(O_2C(CH_2)_2H_3)_4$[a,34]	tricl	104.49 ± 0.02	94.12 ± 0.02	92.74 ± 0.02
$Cu_2(O_2C(CH_2)_6CH_3)_4$[34]	tricl	110.50	95.10	92.40
$Cu_2(O_2C(CH_2)_8CH_3)_4$[34]	tricl	98.60	94.60	97.10

[a] Data from single crystal X-ray diffraction measurements (unit cells have been reoriented to correspond to the unit cell convention of the diffraction patterns, $a > b > c$). [b] Crystallized from a neat melt. [c] Crystallized from hydrocarbon solvent. [d] Triclinic. [e] Body-centered orthorhombic.

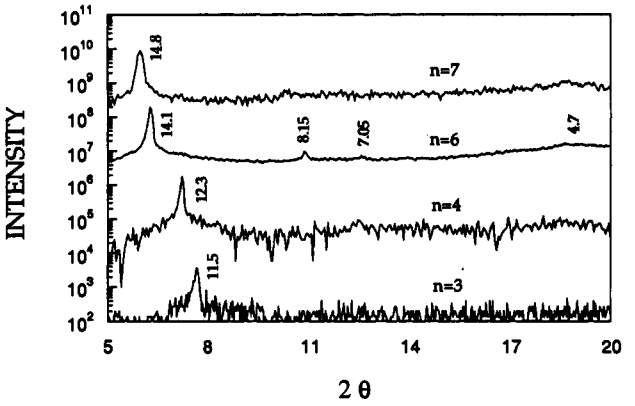

Figure 10. X-ray diffraction pattern obtained for $Mo_2(O_2C(CH_2)_nCH_3)_4$ compounds in the mesophase (n = 3, 4, 6, and 7 as indicated). Numbers next to peaks indicate the corresponding d-spacing in angstroms. Successive curves are offset for clarity of presentation.

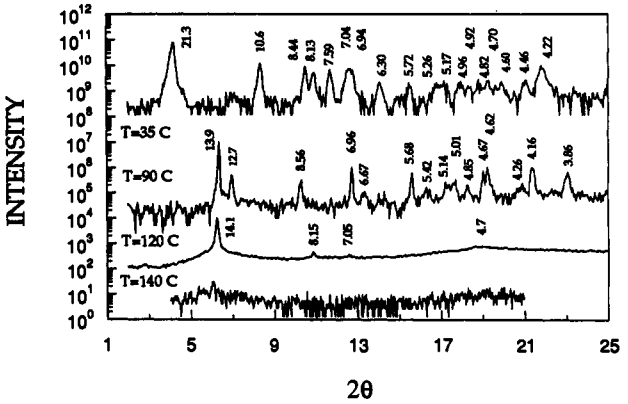

Figure 11. Variable temperature XRD of $Mo_2(O_2C(CH_2)_6CH_3)_4$. These data show clear evidence for a solid–solid phase transition, followed by a transition to a hexagonally packed mesophase, and finally a transition to an isotropic liquid. The temperature given in the figure may differ from the actual sample temperature by as much as 5 °C. As in Figure 10, d-spacings are given in angstroms and the curves have been offset vertically for clarity of presentation.

Table 5. Intercolumnar Separations for Certain $M_2(O_2CR)_4$ Compounds in the Mesophase

$Mo_2(O_2C(CH_2)_nCH_3)_4$	intercolumnar distance (Å)
n = 3	13.3
n = 4	14.2
n = 6	16.3
n = 7	17.1

coherence length along the columns of less than 30 Å. Thus for our samples significant disorder remains along the columnar direction, and the appropriate classification is D_{hd}. The structure of this sample is thus very similar to that reported for other bimetallic mesophases.[46] We assume that a similar arrangement holds for n = 3, 4, and 7, although in these cases the data were too noisy for the smaller peaks to be observed.

A representative example of the diffraction patterns seen upon heating a sample from room temperature through the mesophase is given in Figure 11, for the compound where n = 6. At room temperature the pattern is that of the triclinic phase. By 90 °C the sample transforms into a different solid phase, which subsequently changes to the mesophase by 100 °C. Heating to 145 °C then produces the isotropic liquid.

It is worth mentioning at this point that the triclinic phase appears to be metastable at room temperature for $Mo_2(O_2C(CH_2)_6CH_3)_4$. If this compound is prepared via crystallization from a hydrocarbon solvent, it exists in a body-centered orthorhombic structure (BCO, a = 25.66 Å, b = 16.04 Å, and c = 14.05 Å), which transforms directly into the mesophase upon heating. However, if a sample is prepared via solidification from the isotropic liquid, it forms in the triclinic phase. As noted above, upon heating this triclinic phase transforms into a different solid (one with an X-ray pattern similar to, but slightly different from, the BCO phase) just before reaching the transition to the mesophase. This behavior is similar to the observations previously noted regarding the melt processing of $Mo_2(S_2C\text{-}n\text{-}C_7H_{15})_4$. However, in this case the solid–solid transition appears in DSC measurements on premelted samples only as a small shoulder on the large peak associated with the nearby transition into the mesophase. Melt and solution processing of the compound where n = 7 also produce distinct phases, although in this case solution processing leads directly to the triclinic phase, whereas melt processing forms a phase of apparently higher symmetry whose pattern we have thus far been unable to index.

Molecular Structure of $W_2(O_2C(CH_2)_2CH_3)_4$. As a means of examining the packing of the $[M_2]_\infty$ chains in the solid state, we determined the structure of the butyrate derivative of ditungsten, which, as noted in the Synthesis section, may be obtained in a crystalline form suitable for study by single crystal X-ray crystallography. The related molybdenum compound is presumed to have analogous packing on the basis of the similarity of the cell parameters determined by XRD powder patterns. However, it failed to yield crystals suitable for single crystal studies.

In the space group $P\bar{1}$, there is one unique molecule with a crystallographically imposed center of inversion present in the unit cell. A view of the molecule giving the atom numbering scheme is shown in Figure 12. A summary of crystal data is given in Table 6, and atomic coordinates are given in Table 7. Selected bond distances and angles are given in Table 8.

The molecule shows, as expected for a W–W carboxylate, the typical paddle-wheel type $M_2(O_2C)_4$ core with W–W = 2.194(3) Å and W–O = 2.085(16) Å. The weak intermolecular $W_2\cdots O$

(46) Lai, C. K.; Serrette, A. G.; Swager, T. M. *J. Am. Chem. Soc.* **1992**, *114*, 7948.

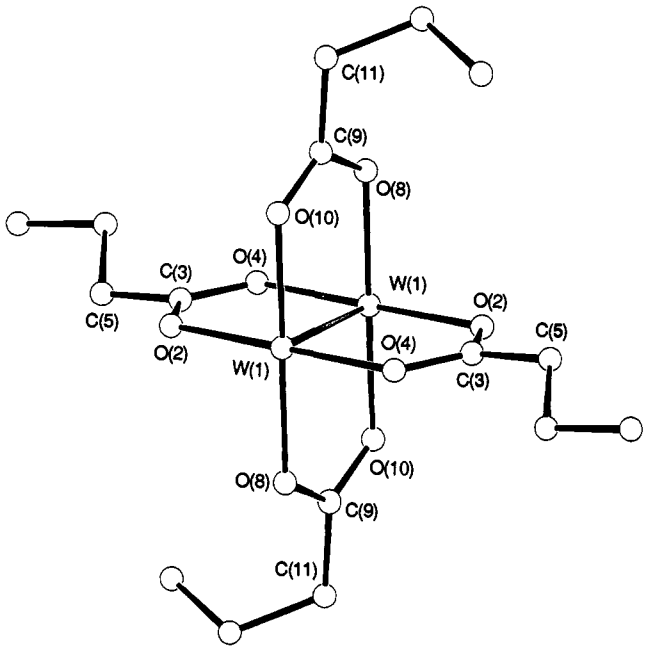

Figure 12. Ball-and-stick drawing of the $W_2(O_2C(CH_2)_2CH_3)_4$ molecule giving the atom numbering scheme used in Tables 7 and 8.

Table 6. Summary of Crystal Data

empirical formula	$C_{16}H_{28}O_8W_2$
color of crystal	orange
crystal dimensions (mm)	0.204 × 0.088 × 0.290
space group	$P\bar{1}$
cell dimensions	
T (°C)	−171
a (Å)	8.867(9)
b (Å)	10.934(14)
c (Å)	5.563(6)
α (deg)	100.01(4)
β (deg)	108.02(3)
γ (deg)	79.58(4)
Z (molecules/cell)	1
V (Å^3)	500.40
d_{calcd} (g/cm^3)	2.376
λ (Å)	0.710 69
MW	716.09
μ (cm^{-1})	117.709
detector-to-sample distance (cm)	22.5
sample-to-source distance (cm)	23.5
av ω scan width at half height	0.25
scan speed (deg/min)	8.0
scan width (deg + dispersion)	2.0
individual background (s)	4
aperture size (mm)	3.0 × 4.0
2θ range (deg)	6–45
total no. of reflections collected	2634
no. of unique intensities	1299
no. with $F\sigma$ 0.0	1285
no. with $F\sigma$3.0(F)	1217
$R(F)$	0.0639
$R_w(F)$	0.0636
goodness of fit for the last cycle	4.236
maximum δ/σ for last cycle	0.05

distance is 2.671(16) Å. This is barely a bond in terms of W–O distances of known compounds, but it is sufficient to cause the ordering in the solid state. (It is insufficiently strong to allow access to the mesophase, as has been noted earlier. See Table 2 for a comparison of Δ(M–O) in related complexes where M = Cu, Rh, Ru, Cr, Mo and W.) The observed structure is closely related to that found for $W_2(O_2CCH_2CH_3)_4$.[27]

Each $W_2(O_2C(CH_2)_2CH_3)_4$ molecule is placed at the corner of the unit cell, and this leads to parallel infinite chains of $W_2(O_2C(CH_2)_2CH_3)_4$ molecules. The M–M axes are thus all aligned, and the angle between the M–M axis and the polymeric growth axis is 32.84°. A packing diagram of two unit cells is shown in Figure 13.

Table 7. Fractional Coordinates and Isotropic Thermal Parameters for $W_2(O_2CCH_2CH_2CH_3)_4$[a]

atom	10^4x	10^4y	10^4z	B_{iso}
W(1)	10 083(1)	540(1)	1882(2)	12
O(2)	9506(17)	−966(14)	3094(29)	17
C(3)	9294(26)	−2037(22)	1536(40)	17
O(4)	9344(17)	−2086(14)	−721(29)	17
C(5)	9050(27)	−3094(21)	2501(41)	17
C(6)	8072(27)	−4040(22)	556(43)	19
C(7)	7885(32)	−5114(24)	1771(48)	27
O(8)	12 482(18)	−156(16)	3227(30)	23
C(9)	13 130(25)	−1011(20)	1632(41)	19
O(10)	12 325(17)	−1277(15)	−623(30)	20
C(11)	14 764(28)	−1551(23)	2678(44)	21
C(12)	15 089(27)	−2083(21)	5189(45)	20
C(13)	14 113(31)	−3118(23)	4970(49)	27

[a] See Figure 12 for atom numbering scheme.

Table 8. Selected Bond Distances (Å) and Bond Angles (deg) for $W_2(O_2CCH_2CH_2CH_3)_4$[a]

A	B	distance
W(1)	W(1)	2.194(3)
W(1)	O(2)	2.081(15)
W(1)	O(4)	2.104(15)
W(1)	O(8)	2.072(15)
W(1)	O(10)	2.085(15)
W(1)	O(2)′	2.671(16)

A	B	C	angle
W(1)	W(1)	O(2)	90.0(4)
W(1)	W(1)	O(4)	91.1(4)
W(1)	W(1)	O(8)	91.6(4)
W(1)	W(1)	O(10)	90.0(4)
O(2)	W(1)	O(4)	178.8(6)
O(2)	W(1)	O(8)	88.9(6)
O(2)	W(1)	O(10)	91.4(6)
O(4)	W(1)	O(8)	91.4(6)
O(4)	W(1)	O(10)	88.3(6)
O(8)	W(1)	O(10)	178.4(6)
W(1)	O(2)	C(3)	120.1(14)
W(1)	O(4)	C(3)	119.8(14)
W(1)	O(8)	C(9)	117.4(13)
W(1)	O(10)	C(9)	120.8(14)

[a] See Figure 12 for atom numbering scheme.

While each molecule has a center of inversion, the arrangements of the *n*-alkyl side chains fall into two sets, as is seen in Figures 12 and 13.

We propose that this structure provides a model for the packing of longer *n*-alkyl carboxylates in that they all adopt an infinitely laddered structure with parallel chains of $[M_2]_\infty$ units and that the alkyl chains are meshed in two different ways (akin to that revealed in Figure 13). This arrangement results in the cell parameters $a \neq b$, while the c parameter remains essentially invariant. Similar packing was observed for $Cu_2(O_2C(CH_2)_6CH_3)_4$ and $Cu_2(O_2C(CH_2)_8CH_3)_4$[34] as depicted in Figure 14. The cell parameters for both compounds are listed in Tables 3 and 4.

NMR Studies. An obvious point of interest is how molecules in liquid crystalline phases align in magnetic and electric fields. The alignment of organic mesophases by applied fields is of fundamental importance in LC technology. We would expect that in any application of metallomesogens the alignment and the switching time would be similarly relevent. Since the Mo≡Mo bond has such a large anisotropy in its magnetic susceptibility (compare −8000 × 10^{-36} m^3/molecule with −340 × 10^{-36} m^3/molecule for ethyne), it should be extremely sensitive to applied fields. The free energy of alignment due to coupling

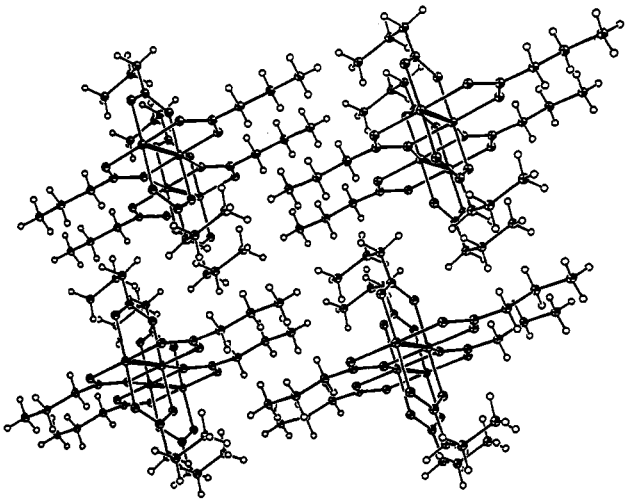

Figure 13. Two unit cells of the $W_2(O_2C(CH_2)_2CH_3)_4$ structure viewed approximately along the c axis. This view emphasizes how in the solid state there are infinite chains, of W_2 units weakly associated by W···O intermolecular interactions and shows the packing of the n-propyl groups between these W_2 chains.

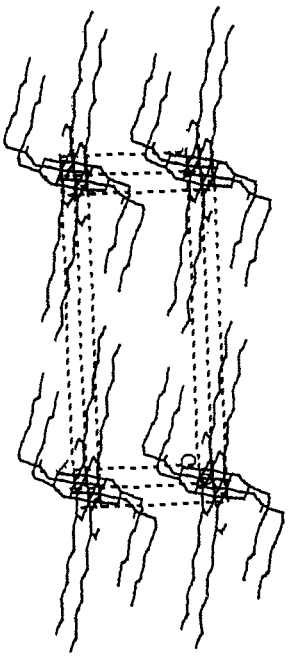

Figure 14. Packing diagram of $Cu_2(O_2C(CH_2)_6CH_3)_4$ showing the similarity with the $W_2(O_2C(CH_2)_2CH_3)_4$ shown in Figure 13. The diagram was generated from the atomic coordinates given in ref 34c.

to a magnetic field can be expressed as eq 6[47]

$$G = -{}^1/_6\Delta\chi\mathbf{B}_0{}^2(3\cos^2\theta - 1) \qquad (6)$$

where $\Delta\chi = \chi_\parallel - \chi_\perp$ is the anisotropy of the magnetic susceptibility, $\mathbf{B}_0$ is the strength of the external magnetic field, and θ is the angle between the director (typically taken as the long axis of a rodlike molecule or the symmetry axis of a disklike molecule) and $\mathbf{B}_0$. Thus, for $\Delta\chi > 0$, the free energy is minimized for alignment parallel to the field, and for $\Delta\chi < 0$, alignment perpendicular to the field should be preferred. Equation 6 refers to single molecules; alignment in the bulk is induced by a similar mechanism.[48] Because the anisotropy of the magnetic susceptibility of the Mo–Mo bond is negative,[13b] taking $\chi_\parallel$ as the magnetic susceptibility along the M–M bond, we would expect alignment of the Mo–Mo axes perpendicular to the applied magnetic field.

(a) Molybdenum-95 NMR Studies. Mo–Mo-containing compounds yield the most deshielded resonances known for ^{95}Mo nuclei, typically 3225 to 4150 ppm (relative to MoO_4^{2-} at $\delta = 0$). In THF, $Mo_2(O_2C(CH_2)_6CH_3)_4$ gave a singlet at 3685 ppm with $\nu_{1/2}$ of 2230 Hz, similar to those seen for other $Mo_2(O_2CR)_4$ compounds with shorter alkyl chains.[49] The line width is about twice as large as those found in the earlier study.[49] From the line width and the reasonable assumption that $T_1 = T_2$ for this system, a relaxation time for the molybdenum spins of $T_1 = 143$ μs can be estimated. The large quadrupole moment of ^{95}Mo and the electronically asymmetric environment at the metal nuclei created by the quadruple bond lead us to expect that the quadrupole coupling constants should be large and will dominate the relaxation of the ^{95}Mo spins. Considering also the effect of solvent viscosity on the relaxation, Shehan *et al.* estimated quadrupole couplings e^2qQ of 12.5 and 11.2 MHz in the tetraacetate and the tetrabutyrate compounds, respectively, and effective molecular correlation times of 11 and 35 ps.[49] Since the Mo_2^{4+} tetrabutyrate and tetraoctanoate are so similar, we assume $e^2qQ = 11.2$ MHz for $Mo_2(O_2C(CH_2)_6CH_3)_4$. That leaves the molecular correlation time to account for our observed line width: from the line width and the estimated e^2qQ, a correlation time of 60 ps, somewhat longer than that found for the butyrate, was calculated. This increase is entirely reasonable, given the increased length of the hydrocarbon chain.

(b) Macroscopic Alignment from ^{95}Mo NMR Spectra. Because both the director of the $Mo_2(O_2C(CH_2)_6CH_3)_4$ molecule and the primary component of the ^{95}Mo quadrupole coupling tensor are coincident with the metal–metal bond, molybdenum NMR should be a pertinent probe of the alignment of the liquid crystal phase in a magnetic field. In principle, even intermolecular Mo_2-to-Mo_2 distances could be determined. The orientational dependence of the spectrum can be predicted from the formalism outlined by Goldman *et al.*[50] Because ^{95}Mo is a spin $^5/_2$ particle, we expect a five-line spectrum for either parallel or perpendicular alignment. For the director parallel to the field, and with the above estimate for e^2qQ, a symmetric spectrum with lines at ±3.36, ±1.68, and 0 MHz, of intensity ratio 5:8:9, respectively, relative to the Larmor frequency of 30 MHz, was calculated. If the Mo–Mo axis is perpendicular to the applied field, the symmetry is broken and the signals should appear at –1.66, –0.87, –0.043, 0.81, and 1.70 MHz, in a similar intensity pattern, namely 5:8:9:8:5, respectively.

We searched carefully for these patterns by heating a pure sample of $Mo_2(O_2C(CH_2)_6CH_3)_4$ to 150 °C and cooling it slowly in an 11.7-T field to the liquid crystal phase. We were unsuccessful in obtaining spectra, presumably because of the large broadening and short relaxation times that are a consequence of the large quadrupole coupling. The broadening would be the most significant problem, as even small deviations from complete alignment would translate into substantial line broadening in the NMR spectrum.

(c) ^{13}C NMR Studies. The carboxylate carbons in $Mo_2(O_2C(CH_2)_6CH_3)_4$ can be thought of as being bound in five-membered rings including also the two molybdenum atoms and the two oxygen atoms. These rings are rather rigid against puckering, and so NMR spectra of the carbons contain information about the alignment of the metal–metal bond.

The ^{13}C NMR spectra of $Mo_2(O_2C(CH_2)_6CH_3)_4$ in solution and as a neat isotropic liquid (at 160 °C) show that the carboxylate carbon chemical shift is 184 ± 1 ppm, while the other seven carbons lie in the range from 12 to 36 ppm. Thus it is easy to study the carboxylate carbons without interference. Figure 15a shows the NMR spectrum of a sample of $Mo_2(O_2C(CH_2)_6CH_3)_4$

(47) Emsley, J. W.; Lindon, J. C. *NMR Spectroscopy Using Liquid Crystal Solvents*; Pergamon Press: New York, 1975.

(48) (a) Levelut, A. M.; Hardouin, F.; Gasparoux, H.; Destrade, C.; Tinh, N. H. *J. Phys.* **1981**, *42*, 147. (b) Dekker, A. J. *Can. J. Phys.* **1987**, *65*, 1185.

(49) Shehan, B. P.; Kony, M.; Brownlee, R. T. C.; O'Connor, M. J.; Wedd, A. G. *J. Magn. Reson.* **1985**, *63*, 343.

(50) Goldman, M.; Grandinetti, P. J.; Llor, A.; Olejniczak, Z.; Sachleben, J. R.; Zwanziger, J. W. *J. Chem. Phys.* **1992**, *97*, 8947.

enriched to 99% in ^{13}C at the carboxylate position, in a field of 4.68 T at 160 °C. When this sample is cooled slowly (0.5 deg/min) to 120 °C in the field, the spectrum shown in Figure 15b results from the mesophase. The peak is somewhat broadened, and, most importantly, is shifted upfield to 169 ± 2 ppm.

In order to understand these spectra, it is necessary to consider the elements of the chemical shift tensor of the carboxylate carbon and the orientation of the tensor with respect to the molecule. Figure 16 shows the spectrum of the ^{13}C-enriched polycrystalline sample at room temperature prior to heating. The spectrum was obtained with cross-polarization followed by high-power proton decoupling. Signals from the methyl and methylene carbons are seen, weakly, upfield. The three principal values of the chemical shift tensor of the carboxylate carbon can be read off Figure 16 as σ_{zz} = 124 ± 3 ppm, σ_{xx} = 220 ± 3 ppm, and σ_{yy} = 209 ± 1 ppm.

A variety of carboxylic acids and carboxylates have been studied by single-crystal NMR spectroscopy, and the principal values and orientations of the chemical shift tensors of the carboxylate carbons have been determined.[51] When the C–O bond lengths are equivalent (as in the present case), it is found that the tensors are oriented as shown in **VI**.

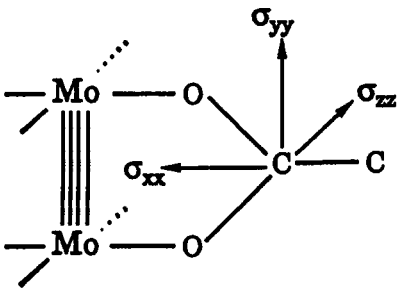

VI

The most shielded element [σ_{zz} in $Mo_2(O_2C(CH_2)_6CH_3)_4$] is normal to the O–C–O plane, and the most deshielded (σ_{xx}) is parallel to the C–C bond. Compared to other carboxylates, in $Mo_2(O_2C(CH_2)_6CH_3)_4$, σ_{xx} is shifted upfield by about 20 ppm, while σ_{zz} is shifted downfield by about the same amount and σ_{yy} is shifted downfield by about 35 ppm. These shifts can be understood qualitatively by taking into account the magnetic susceptibility and proximity of the M–M bond.[52] By using the standard analysis, the metal–metal bond contributes $-\chi_\perp/4\pi R^3$ to σ_{zz}, $2\chi_\perp/4\pi R^3$ to σ_{xx}, and $-\chi_\parallel/4\pi R^3$ to σ_{yy}, where R is the distance from the center of the metal–metal bond to the carbon atom. By assuming $\chi_\perp$ and $\chi_\parallel$ to be negative, as is almost always the case, we would predict the metal–metal bond to shield the carbon atom in the xx direction and to deshield it in the other directions. Moreover, using R = 2.64 Å and $\chi_{\perp,\parallel} \approx (10^3\text{–}10^4) \times 10^{-36}$ m^3/molecule, the contributions to the shifts are in the range of 4–40 ppm. This analysis provides the correct sense and order of magnitude of excess shielding for the three tensor components.

With the above assignment of the orientation, we can interpret the data on $Mo_2(O_2C(CH_2)_6CH_3)_4$ in the different phases. First, the isotropic average of the three tensor elements from the powder pattern is σ = 184 ± 1.5 ppm, which agrees well with the value observed in the isotropic liquid of 184 ± 1 ppm. The spectrum of the liquid crystal shows by virtue of its single sharp peak that the sample is either aligned such that one of the principal axis directions is parallel to the applied field or aligned and rotating such that two or more of the tensor elements are averaged together. Since the spectral line does not fall near any of the tensor elements, the first alternative can be discarded immediately. Among the possible alignments thus rejected is that of the metal–metal bond parallel to the magnetic field. The spectrum is uniquely explained, however, by assuming that the bond is aligned perpendicularly to the applied field, and that the molecule rotates rapidly about this direction. In this case, one would observe the average of σ_{xx} and σ_{zz}, which from our solid-state measurements is estimated to be 172 ± 2.1 ppm, in satisfactory agreement with the spectrum of the liquid crystal (169 ± 2 ppm). Thus, in the mesophase, $Mo_2(O_2C(CH_2)_6CH_3)_4$ is aligned with the metal–metal bond perpendicular to the applied magnetic field, as we previously anticipated from the negative anisotropy observed in other Mo–Mo bonds. The rapid rotation about the M–M axis is consistent with the C_4 rotations depicted in Figure 4.

Concluding Remarks. Our studies on group VI dimetal tetracarboxylates have shown the importance of M_2···O interactions in the liquid crystalline phase. For M = Cr, whose axial interactions are comparable to those in late transition-metal tetracarboxylates, the liquid crystal phase does not clear before decomposing. For M = Mo, the axial interactions are weakened enough to be overcome at temperatures before decomposing but strong enough to allow access to the mesophase. For M = W, the interactions are so weak that no mesophase occurs. When thiocarboxylates are used, replacing M_2···O with M_2···S interactions, no mesophases are observed.

Thus, the phase diagram of $Mo_2(O_2CR)_4$ complexes is unique, allowing both solid-to-liquid crystal and liquid crystal-to-liquid transitions to be studied. Previous studies on $Cu_2(O_2CR)_4$ complexes[30] have shown that longer alkyl chains increase the solid-to-liquid crystal transition temperature. For $Mo_2(O_2CR)_4$, such a trend is not observed due to the decrease in liquid crystal-to-liquid transition temperatures and the lack of mesophase behavior for long-chain alkyls. These trends indicate that the alkyl chains play some role in each transition.

We modified the ligand chains to determine their role, finding that it is quite complex. Use of fluorinated alkyls with M = Mo and Cr stabilizes the solid phase at higher temperatures, while with M = W the solid phase is prone to thermal decomposition. The liquid crystal-to-liquid transition occurred only for M = Mo and was raised compared to the non-fluorinated complex, suggesting that the M_2···O interaction was strengthened by the electron-withdrawing ligand.

Incorporation of a methyl branch on the carbon adjacent to the carboxylate carbon for M = Mo lowers the solid-to-liquid crystal transition temperature, apparently disrupting the interactions between chains but does not change the liquid crystal-to-liquid transition. However, more studies need to be carried out to understand fully the role of branching. In contrast to our study, introduction of an ethyl branch at the same position on a long alkyl chain for M = Cu[39] increases the solid-to-liquid crystal temperature.

The presence of -C_6H_4- and -C_6H_4O- groups adjacent to the carboxylate carbon stabilizes the solid state for both M = Mo and Cr. For M = Mo, the solid-state phases exist at temperatures over 75 °C higher than the clearing temperature for the alkyl analogue. The -C_6H_4O- unit has been used with M = Cu[53] and Rh[54] tetracarboxylates, having little effect on the thermal behavior of the Cu compound but stabilizing the solid state by *ca.* 50 °C for Rh. The clearing temperatures for both are lowered below decomposition. Evidence for a smectic phase has been seen for M = Cu.

Although the effects of varying ligands differ for different metal systems and are not well understood, the core interactions

(51) (a) Veeman, W. S. *Prog. NMR Spectrosc.* **1984**, *16*, 193. (b) Duncan, T. M. *J. Phys. Chem. Ref. Data* **1987**, *16*, 125.

(52) Lynden-Bell, R. M.; Harris, R. K. *Nuclear Magnetic Resonance Spectroscopy*; Appleton-Century-Crofts, New York, 1969.

(53) Ibn-Elhaj, M.; Guillon, D.; Skoulios, A.; Giroud-Godquin, A.-M.; Maldivi, P. *Liq. Cryst.* **1992**, *11*, 731.

(54) Barberá, J.; Esterueles, M. A.; Levelut, A. M.; Oro, L. A.; Serrano, J. L.; Solo, E. *Inorg. Chem.* **1992**, *31*, 732.

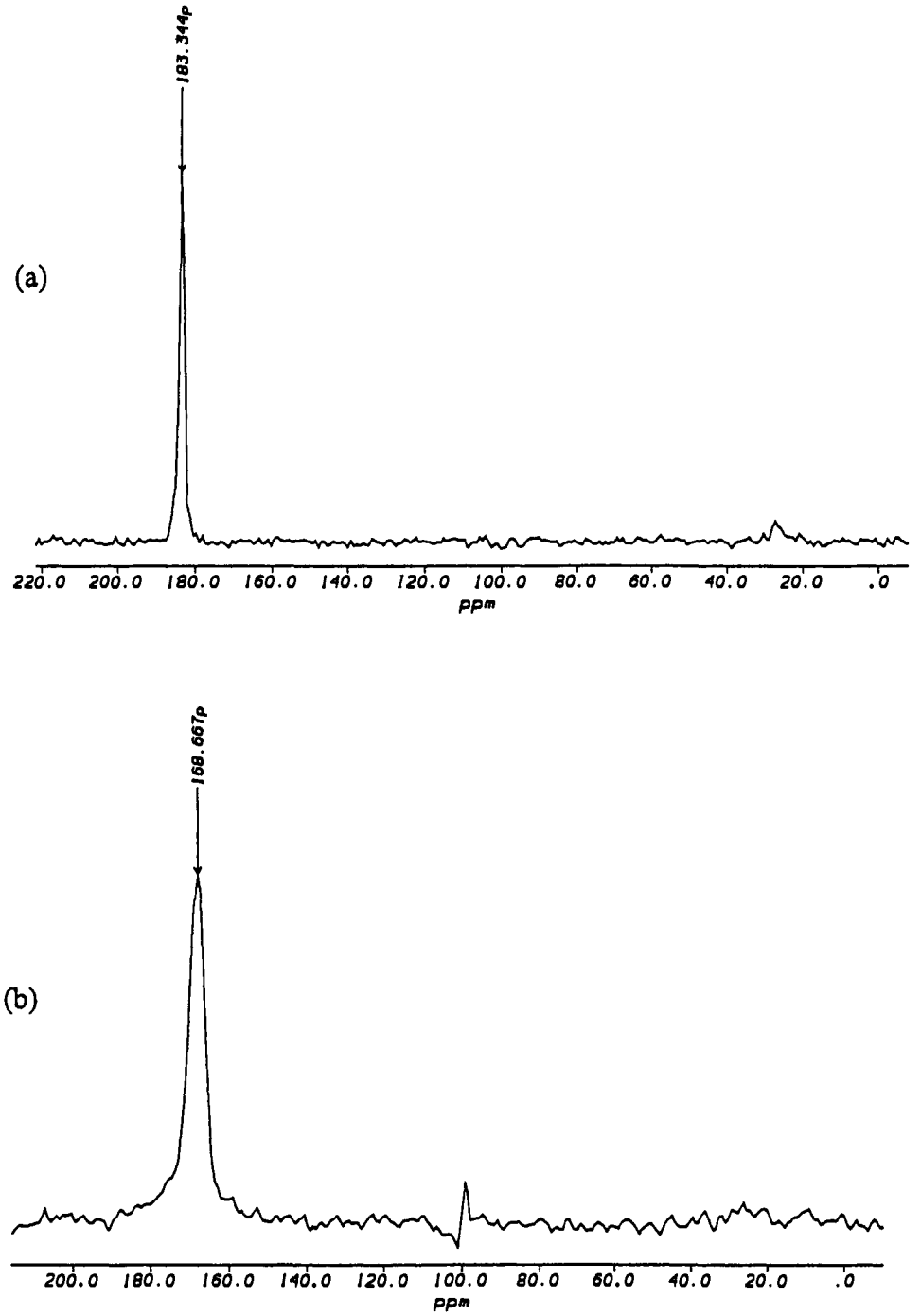

Figure 15. ^{13}C NMR spectra of $Mo_2(O_2{}^{13}C(CH_2)_6CH_3)_4$ in the isotropic liquid state (a, top) and in the mesophase (b, bottom).

are similar. Polarized microscopy, X-ray diffraction, and ^{13}C NMR studies reported here indicate that $Mo_2(O_2CR)_4$ systems behave like M = Cu and Rh systems. For M = Cu[55] and Rh,[56] EXAFS studies have shown that the $M_2\cdots O$ interactions are maintained in the mesophases. Intracolumnar stacking distances shorter than those in the solid state indicated that their hexagonal mesophases resulted from a crankshaft or north–south–east–west arrangement. Our polarized microscopy and VT X-ray diffraction studies on M = Mo showed the hexagonal symmetry of the mesophases, while the latter also gave an intracolumnar stacking distance of 4.7 Å.

The kinetic lability of the $Mo_2\cdots O$ intermolecular interactions (bonds) is fast on the NMR time scale in the mesophase since there is rapid rotation about the Mo–Mo axes. This leads to the averaging of σ_{xx} and σ_{zz} chemical shift tensors for the $O_2{}^{13}C$ carbon atoms when the mesophase is oriented in a magnetic field. At a distance of 2.64 Å, one would certainly expect the $Mo_2\cdots O$ interactions to be extremely weak, on the order of a few kilocalories per mole at most. Kinetic studies on the $Mo_2(aquo)^{4+}$ ion led Sykes *et al.*[57] to suggest that the axial site exchange of H_2O molecules was close to the rate of diffusion. Thus the rate of switching may be quite fast for $Mo_2(O_2CR)_4$ compounds in the mesophase.

Further studies of the optical and physical properties of these highly anisotropic and hyperpolarizable metallomesogens are planned.

(55) (a) Maldivi, P.; Guillon, D.; Giroud-Godquin, A.-M.; Marchon, J.-C.; Abied, H.; Dexpert, H.; Skoulios, A. *J. Chem. Phys.* **1989**, *86*, 1651. (b) Abied, H.; Guillon, D.; Skoulios, A.; Dexpert, H.; Giroud-Godquin, A.-M.; Marchon, J.-C. *J. Phys.* (*Paris*) **1988**, *49*, 345.

(56) Ibn-Elhaj, M.; Guillon, D.; Skoulios, A.; Maldivi, P.; Giroud-Godquin, A. M.; Marchon, J.-C. *J. Phys.* (*Paris*) *II* **1992**, *2*, 2237.

(57) Finholt, J.; Leupin, P.; Sykes, A. G. *Inorg. Chem.* **1983**, *22*, 3315.

Figure 16. ^{13}C NMR spectrum of $Mo_2(O_2{}^{13}C(CH_2)_6CH_3)_4$ recorded as a polycrystalline sample and revealing the ^{13}C chemical shift tensors σ_{xx}, σ_{yy}, and σ_{zz} for the carboxylate carbon.

Experimental Section

All reactions were carried out using standard Schlenk techniques with dry, oxygen-free solvents. $Mo(CO)_6$, $CrCl_2$, and organic acids were purchased from commercial sources. 1,2-$W_2Et_2(NMe_2)_4$,[58] $Mo_2(O_2CMe)_4$,[59] $W_2(O_2CMe)_4$,[26] and the salts of organic acids were prepared according to the literature procedures.

^1H NMR spectra were recorded on a Varian XL300 spectrometer at 300 MHz, and ^{19}F NMR spectra were recorded on a Nicolet NT360 spectrometer at 340 MHz in oxygen-free solvents. All ^1H NMR chemical shifts are reported in parts per million (ppm) relative to the protio impurity resonances.

^{95}Mo NMR was performed on a Bruker AM500 spectrometer with ν_0 = 32.6 MHz. Spectra were obtained with an acquisition delay of 1 s, with typically 5000 scans.

^{13}C NMR spectra were acquired on a sample of dimolybdenumtetraoctanoate enriched to 99% at the carboxylate carbon [$Mo_2(O_2C^*(CH_2)_6CH_3)_4$]. The ^{13}C spectra were taken on a Nicolet NT200 spectrometer with ν_0 = 50.3 MHz. The spectrum of the static solid, sealed in an evacuated glass tube, was obtained using cross-polarization followed by high-power decoupling. First, the spectrometer was adjusted for cross-polarization using hexamethylbenzene. The ^{13}C spectrum of dimolybdenumtetraoctanoate was then acquired with a contact time of 10 ms, an acquisition delay of 5 s, and high-power decoupling of 90 W. Typically 3000–4000 scans were acquired. Spectra of the isotropic liquid were obtained by heating the sample to 160 °C. On the order of 100 scans were acquired with a 3-s delay by using a single-pulse acquisition with high-power decoupling. The spectrum was unchanged by decoupling. The spectrum of the liquid crystal was obtained by cooling the sample in the magnetic field from 160 °C to 120 °C at a rate of 0.5 deg/min. The same parameters were used in the liquid spectrum, including high-power decoupling. In this case, decoupling was required in order to suppress broadening from the protons.

DSC measurements were performed on a duPont Instruments 910 differential scanning calorimeter. The hermetically sealed samples (Al cells) were heated under a N_2 or He gas flow at a heating rate of 5 deg/min.

Variable temperature X-ray patterns were collected by using a Scintag XDS2000 $\theta - \theta$ goniometer fitted with a Model HT2000C high-temperature stage. In order to protect against degradation of the sample, the stage enclosure was continuously purged with purified He gas, and scan rates of 1–2 deg/min were used over an angular range of up to 20° (in 2θ). As a result, each sample was typically at elevated temperatures for no more than 2 h in an inert atmosphere. In one case, in order to attain greater statistical accuracy, data were collected over a 12-h period at a single temperature. In this case, slight discoloration of the sample was noted after the run, but no evidence of significant degradation was evident in an X-ray measurement of the solid at room temperature. To ensure that the aluminum cuvette contained sufficient sample for measurements of the mesophase, the starting powder material was loaded into the cuvette while the latter was held above the melting point of the sample material by using a hot plate in a nitrogen-filled glove box. Thus, for instance, the room temperature solid phase seen in Figure 11 is the metastable (melt processed) triclinic phase. The cuvette was placed on the Pt–Ir heating element of the hot stage with minimal exposure to the atmosphere (on the order of 15 min, including the time taken to purge the sample volume of the hot state). The temperature was determined by a Pt/Pt–Rh (10%) thermocouple attached directly to the heating element; the actual sample temperature could differ from this by as much as 5 °C over the temperature range considered.

Polarized Microscopy. The principal apparatus used for heat-treating the samples was a Linkham controlled atmosphere hot stage. Specimen temperature was regulated with a programmed control system connected to the furnace, capable of multiple heating/cooling ramps at various rates.

The microscopy studies were conducted with a Zeiss Universal microscope, equipped with a 16× UD Achromat objective and an Optivar 1.25× lens. A quartz halogen lamp was used for reflected Kohler illumination. Birefringence was observed using two Zeiss plane-polarizing filters oriented as fully-crossed polars.

In our experiments, the hot stage was heated or cooled at the rate of 5 deg/min.

Synthesis. $Mo_2(O_2C(CH_2)_nCH_3)_4$. Diglyme was added to mixtures of white solid $Mo(CO)_6$ and 3 equiv of necessary acids together with *ca.* 3 mL of THF. The mixtures were stirred while being refluxed for *ca.* 6 h. After cooling, the diglyme was removed by either vacuum distillation or filtration, and yellow crystals of $Mo_2(O_2C(CH_2)_nCH_3)_4$ were obtained by recrystallization from toluene. Excess hexane was used to wash off any remaining acid. Average yield was *ca.* 60%. The compounds were characterized by ^1H NMR after being dried under dynamic vacuum. ^1H NMR data: n = 2 (acetone-d_6) δ 1.01 (t, 3H), 1.83 (m, 2H), 2.85 (t, 2H); n = 3 (py-d_5) δ 0.88 (t, 3H), 1.47 (sxt, 2H), 1.94 (pent, 2H), 3.14 (t, 2H); n = 4 (benzene-d_6) δ 0.95 (t, 3H), 1.38 (m, 4H), 1.89 (t, 2H), 2.83 (t, 2H); n = 5 (benzene-d_6) δ 0.95 (t, 3H), 1.34 (m, 6H), 1.90 (t, 2H), 2.88 (t, 2H); n = 6 (benzene-d_6) δ 0.95 (t, 3H), 1.32 (m, 8H), 1.92 (t, 2H), 2.89 (t, 2H); n = 7 (benzene-d_6) δ 0.93 (t, 3H), 1.31 (m, 10H), 1.91 (m, 2H), 2.94 (m, 2H); n = 8 (benzene-d_6) δ 0.93 (t, 3H), 1.30 and 1.34 (overlapping mult, 12H), 1.90 (m, 2H), 2.93 (m, 2H).

$W_2(O_2C(CH_2)_6CH_3)_4$. $HOOC(CH_2)_6CH_3$ (0.189 g, 1.31 mmol) was added to the slurry of $W_2(O_2CMe)_4$ (0.198 g, 0.33 mmol) in 25 mL of toluene at room temperature. A dark yellow-brown solution was formed upon stirring. The azeotropic mixture of toluene and acetic acid was removed under vacuum repeatedly. Yellow solid was isolated upon cooling the solution to –40 °C. The solid was recrystallized from ether at –78 °C, forming thin yellow-orange needles, and dried under vacuum at room temperature for 10 h. Yield was 40%. ^1H NMR (benzene-d_6): δ 0.92 (t, 3H), 1.31 (m, 8H), 1.86 (pent, 2H), 3.23 (t, 2H).

$W_2(O_2C(CH_2)_2CH_3)_4$. To the solution of 0.1 g (0.17 mmol) of $W_2(NMe_2)Et_2$ in 15 mL of hexane was added 4 equiv (0.108 mL, 0.68 mmol) of butyric anhydride at room temperature. The color immediately changed from yellow to green. Upon further reacting, the color changed again to brownish-yellow. The volume of the solution was reduced, and yellow crystals were obtained upon cooling the reaction media to –40 °C. ^1H NMR (acetone-d_6): δ 0.91 (t, 3H), 1.78 (m, 2H), 3.13 (t, 2H).

$Cr_2(O_2C(CF_2)_6CF_3)_4$. To the blue solution of 0.042 g (0.34 mmol) of $CrCl_2$ in 15 mL of methanol was added 2 equiv of $NaO_2C(CF_2)_6CF_3$ (0.296 g, 0.68 mmol) at room temperature. Purple precipitate formed upon stirring the reaction mixture for 30 min. The precipitate was isolated and dried under vacuum at elevated temperature to remove possible axially ligated solvent molecules. ^1H NMR indicated no signals of starting

(58) (a) Chetcuti, M. J.; Chisholm, M. H.; Folting, K.; Haitko, D. A.; Huffman, J. C.; Janos, J. *J. Am. Chem. Soc.* **1983**, *105*, 1163. (b) Chisholm, M. H.; Haitko, D. A.; Folting, K.; Huffman, J. C. *J. Am. Chem. Soc.* **1981**, *103*, 4046.

(59) Brignole, A. B.; Cotton, F. A. *Inorg. Synth.* **1972**, *13*, 81.

materials or solvents. ^{19}F NMR (CD_2Cl_2): δ −81.22 (s, 3F), −112.60 (br s, 2F), −117.84 (br s, 4F), −121.52 (s, 2F), −121.93 (s, 2F), −124.86 (s, 2F), also decomposition signals at −111.21 (br), −117.83 (br).

$Mo_2(O_2C(CF_2)_6CF_3)_4$. $Mo_2(O_2CMe)_4$ (0.225 g, 0.53 mmol) and $HOOC(CF_2)_6CF_3$ (0.871 g, 2.10 mmol, 4 equiv) were dissolved in 40 mL of toluene and heated to 70 °C. Yellow solid precipitated out of the solution upon stirring at this temperature for 3 h. The azeotropic mixture of toluene and acetic acid was removed under vacuum. The solid was recrystallized from pentane and dried under vacuum. ^1H NMR indicated no signals of starting materials or solvents. ^{19}F NMR (CD_2Cl_2): δ −82.1 (s, 3F), −116.7 (s, 2F), −121.7 (s, 2F), −122.5 (s, 2F), −123.4 (br s, 4F), −126.9 (s, 2F).

$W_2(O_2C(CF_2)_6CF_3)_4$. A solution of 0.411 g (0.99 mmol) of $HOOC(CF_2)_6CF_3$ in 15 mL of THF was added to the slurry of 0.150 g (0.25 mmol, 4 equiv) of $W_2(O_2CMe)_4$ in 25 mL of toluene at room temperature. The solvent was removed, and the dark oily residue was dried under vacuum and redissolved in DME. Yellow solid was isolated upon cooling the solution to −40 °C. The solid was washed with pentane at −20 °C and dried under vacuum at −20 °C for 4 h. ^1H NMR indicated no signals of starting materials or solvents. ^{19}F NMR (CD_2Cl_2): δ −82.17 (S, 3F), −119.48 (s, 2F), −122.50 (s, 2F), −122.86 (s, 2F), −123.57 (s, 2F), −123.60 (s, 2F), −127.12 (s, 2F).

$Cr_2(O_2C(C_6H_4)$-n-$C_7H_{15})_4$ and $Cr_2(O_2C(C_6H_4)O$-n-$C_7H_{15})_4$. To the solution of $CrCl_2$ in methanol was added the solution of $LiO_2C(C_6H_4)(CH_2)_6CH_3$ or $LiO_2C(C_6H_4)O(CH_2)_6CH_3$ in methanol at room temperature. Dark-tan or coffee-color precipitates formed immediately. The precipitates were isolated, washed with methanol, and dried under vacuum for 4 h. ^1H NMR data: $Cr_2(O_2C(C_6H_4)$-n-$C_7H_{15})_4$ (benzene-d_6) δ 0.88 (t, 3H), 1.20 (br m overlapping with other signals, approximately 8H), 1.45 (m, 2H), 2.45 (m, 2H), 6.89 (br m, 2H), 8.23 (br m, 2H); $Cr_2(O_2C(C_6H_4)O$-n-$C_7H_{15})_4$ (benzene-d_6) δ 0.86 (t, 3H), 1.15 (br m, approximately 8H), 1.47 (m, 2H), 3.15 (t, 2H), 3.42 (1, 2H), 6.61 (m, 2H), 8.18 (m, 2H).

$Mo_2(O_2C(C_6H_4)$-n-$C_7H_{15})_4$ and $Mo_2(O_2C(C_6H_4)O$-n-$C_7H_{15})$. $Mo(CO)_6$ was mixed with 4 equiv of p-heptylbenzoic or p-heptoxybenzoic acid. The mixture was refluxed in diglyme for 6 h and, after the color was intensive yellow-orange, the solvent was removed. The yellow solid was recrystallized from toluene at −40 °C, washed with hexane, and dried under vacuum. ^1H NMR data: $Mo_2(O_2C(C_6H_4)$-n-$C_7H_{15})_4$ (benzene-d_6) δ 0.89 (t, 3H), 1.19 (m, 8H), 1.43 (m, 2H), 2.34 (t, 2H), 6.69 (d, 2H), 8.36 (d, 2H); $Mo_2(OOC(C_6H_4)O$-n-$C_7H_{15})_4$ (benzene-d_6) δ 0.88 (t, 3H), 1.18 (m, 8H), 1.51 (m, 2H), 3.02 (d, 2H), 3.48 (t, 2H), 6.71 (d, 2H), 8.40 (d, 2H).

$Mo_2(O_2C(CH_2)_2CH(CH_3)(CH_2)_4CH_3)_4$. $Mo_2(O_2CMe)_4$ (0.200 g, 0.47 mmol) was mixed with 4-methylnonanoic acid (0.322 g, 1.86 mmol, 4 equiv) and 30 mL of toluene was added to the mixture. After the solution was stirred for 3 h at 60 °C, the color became darker yellow. The azeotropic mixture of toluene with acetic acid was removed under vacuum. The dark yellow oily product was isolated, washed with pentane, and dried under vacuum for 3 h. Brownish solid was obtained. ^1H NMR (benzene-d_6): δ 0.94 (t, 3H), 0.97 (d, 3H), 1.31 (doublet overlapping with small multiplets, *ca.* 5H), 1.51 (m, 2H), 1.79 (m, 2H), 2.05 (m, 2H), 2.96 (t, 2H).

$Mo_2(S_2C(CH_2)_nCH_3)_4$, Where n = 2 and 6. $CH_3(CH_2)_nMgBr$ was dissolved in THF and cooled to 0 °C. A 2-fold excess of CS_2 was added dropwise. The color of the solutions immediately turned yellow. Upon stirring of the solution for 30 min at room temperature, the color slowly changed to yellow-orange. The prepared ligands were transferred to the slurry of $Mo_2(O_2CMe)_4$ in THF, causing the color immediately to turn blood-red. The volume of the solutions was reduced, and methanol was added to form bright orange precipitates. The precipitates were isolated, washed with methanol, and dried under vacuum. ^1H NMR data: n = 2 (benzene-d_6) δ 0.88 (t, 3H), 1.35 (m, THF) 1.92 (m, 2H), 3.15 (t, 2H), 3.55 (t, THF); n = 6 (benzene-d_6) δ 0.93 (t, 3H), 1.32 (broad overlapping multiplet, approximately 10H), 2.01 (m, 2H), 3.27 (t, 2H).

Crystallographic Determination of $W_2(O_2C(CH_2)_2CH_3)_4$. General operating procedures and listings of programs have been given previously.[60] A summary of crystal data is given in Table 6. Well-formed orange crystals were present, and a typical crystal was affixed to the end of a glass fiber and transferred to the goniostat, where it was cooled to −171 °C for characterization and data collection.

A systematic search of a limited hemisphere of reciprocal space located a set of diffraction maxima with no symmetry or systematic absences, indicating a triclinic space group. Subsequent solution and refinement confirmed the proper choice to be $P\bar{1}$. Data were collected by using a standard moving crystal, moving detector technique with fixed background counts at each extreme of the scan. Data were corrected for Lorentz and polarization terms, and equivalent data were averaged. Of 1299 unique data collected, 1217 were considered "observed", based on the criterion $F > 2.33\sigma(F)$.

The structure was readily solved by a combination of direct methods (MULTAN78) and Fourier techniques. In spite of the well-defined faces of the crystal, the absorption correction was not as satisfactory as desired, with peaks of up to 3.2 e/Å^3 at the metal site. There is one molecule in the unit cell with a crystallographically imposed center of inversion.

Acknowledgment. We thank the National Science foundation (D.V.B., M.H.C., and J.W.Z.) and the donors of the Petroleum Research Fund (J.W.Z.), administered by the American Chemical Society, for financial support. S.L.T. thanks the Department of Education for a fellowship. The Indiana University Research Facilities Fund and Amoco Research Corporation are gratefully acknowledged for providing the high-temperature XRD and the NT200 NMR spectrometer. We also wish to thank Professor M. D. Hollingsworth and Dr. Stefan Idziak for helpful discussions and Mr. Bob Addleman and Deon Osman for their efforts to obtain ^{95}Mo NMR spectra of the mesophases.

Supplementary Material Available: For $W_2(O_2C$-Pr$)_4$, a listing of anisotropic thermal parameters, and a complete listing of bond distances and angles (3 pages); listing of observed and calculated structure factors (4 pages). This material is contained in many libraries on microfiche, immediately follows this article in the microfilm version of the journal, and can be ordered from the ACS; see any current masthead page for ordering information.

(60) Chisholm, M. H.; Folting, K.; Huffman, J. C.; Kirkpatrick, C. C. *Inorg. Chem.* **1984**, *23*, 1021.